DIPLOMARBEIT

Titel der Diplomarbeit

Seismic signal analysis using polarization attributes and its applications

angestrebter akademischer Grad

Magistra der Naturwissenschaften (Mag. rer.nat.)

Durchgeführt am

Institut für Geodäsie und Geophysik
der Technischen Universität Wien

Verfasserin:	Katharina Doblhoff-Dier
Matrikel-Nummer:	525856
Studienrichtung:	Diplomstudium Geophysik
Betreuer:	Prof. Dr Ewald Brückl
	Mag. Stefan Mertl

Wien, im April 2011

Abstract

Seismic three component data has been available for several decades and it has been known long since that polarization analysis is a powerful method to extract information contained in such data. However, polarization analysis is not widely used in regional seismology and a comprehensive textbook cannot be found. The goal of this work is, therefore, to give a theoretical introduction and a state of the art review of polarization analysis. In the course of this work, several methods were implemented for the open source program SEISMON. The implemented methods were applied to global and regional earthquake data, discussed in detail and then used to fathom the possible use of polarization analysis in the characterization and investigation of short period data. The methods were found to give consistent results, often complementing each other. A major success was achieved by improving the characterization of short period events measured at the land slide in Gradenbach.

Kurzfassung

Seit mehereren Jahrzehnten können und werden bei seismischen Messungen drei Komponenten aufgezeichnet und seit langem ist bekannt, dass Polarisationsanalysen helfen können zusätzliche Informationen aus drei-Komponenten Daten abzuleiten. Dennoch werden Polarisationsanaysen in der regionalen und lokalen Seismologie kaum verwendet und ein umfassendes Lehrbuch fehlt. Es ist daher das Ziel dieser Arbeit die theoretischen Grundlagen der Polarisationsanalyse zu erklären und eine umfassende Zusammenfassung der bisher entwickelten Methoden zu geben. Im Ramen dieser Arbeit wurden mehrere Methoden der Polarisationsanalyse for das open source Programm SEISMON implementiert. Die implementierten Methoden wurden anschließend bei globalen und regionalen Erdbebendaten angewandt und genau analysiert. Dann wurde die mögliche Verwendung der Methoden in der Characterisierung von short period events augelotet. The implementierten Methoden geben konsistente Ergebnisse und/oder kompementieren eindander. Ein wesentlicher Erfolg konnte in der Verbesserung der Characterisierung von short period event von der Hangrutschung in Gradenbach erzielt werden.

Acknowledgments

First, I would like to thank my supervisor, Prof. Ewald Brückel from the technical university of Vienna for many helpful discussions and his encouragement.

I also want to thank Mag. Stefan Mertl, who provided me with sorted and cataloged data from the landslide near Gradenbach. Stefan Mertl also introduced me to his software SEISMON and was very helpful in resolving problems with the software. I also acknowledge his help in improving the user-interface of the methods I implemented in the course of this work.

My thanks also go to my colleague Dipl. Ing. Maria Apoloner for providing me with various scripts making life easier.

Contents

1. Introduction

Digital three component (3C) seismic data has been available for several decades. The recording of 3C data is corner stone for any polarization analysis, since polarization analysis deals with the three-dimensional oscillatory motion of waves. Already in the 1960's [1] it was found that additional information can be extracted from 3C data by using polarization analysis and polarization filtering. Since the 1980's the information contained in 3C data has been exploited in the interpretation of seismic data. Never the less, no comprehensive and known textbooks or reviews can be found dealing with polarization analysis. Also, polarization analysis has not been used routinely in seismology, especially not for regional and local seismic events.

The goal of this work is not only to provide a synopsis of various known polarization analysis methods; it is also meant to give a thorough theoretical background which is necessary to understand the physical meaning of different polarization analysis methods. Most theory is based on optics where polarization attributes have been exploited for a much longer time than in geophysics. This theory background and the necessary extensions thereof for seismic waves is given in Chapter 2. In Chapter 3, I present several different methods of polarization analysis, which were implemented for the signal analysis program SEISMON (see Appendix). The methods were tested and applied to a range of different data types, ranging from teleseismic events over regional earthquakes all the way to microseismic event. The methods presented in Chapter 3, are discussed in detail in Chapter 4, where they are applied to teleseismic events. In Chapter 5, selected methods are applied to regional and microseismic events in order to demonstrate the potential use of polarization analysis in the investigation of microseismic events, as, for example, encountered in the seismic monitoring of landslides.

2. Theory

2.1. Wave Polarization

Wave polarization is a well known concept for transverse waves, such as light waves in an isotropic medium. Although we cannot directly observe the polarization characteristics of electromagnetic waves, already Newton observed that light carries a directional property other than its direction of propagation [2]. Tomas Young later attributed this directional property to the transverse wave component of light [3]. In general,"polarization" refers to the wave's direction of vibration. If a wave is polarized, its oscillating quantity (e.g. the electromagnetic field) has a well defined orientation at each moment in time [4]. We distinguish between different types of polarization: linear polarization, circular polarization and elliptical polarization, where the last named is the most general type and includes the two former as special cases.

2.1.1. Polarization of Transverse Waves

Light waves, i.e. electromagnetic waves, for which the property of polarization was first described, are transverse waves. This means that there is no vector component parallel to the direction of motion. Hence, the field is confined to a plane orthogonal to the ray path. I will explain the concept of polarization for this special case first, before considering the more general case of elastic waves in media, where there is no restriction to the vibrational motion.

Types of Polarization and their Description

A transverse, time-harmonic, monochromatic wave can be written as

$$\vec{E}(\zeta, t) = \begin{pmatrix} A_\xi \cos(\omega t - k\zeta + \phi_\xi) \\ A_\eta \cos(\omega t - k\zeta + \phi_\eta) \end{pmatrix} ,$$

where ξ and η span the plane perpendicular to the direction of motion ζ, A_i are the amplitudes in the i-direction, ω is the angular frequency, t the time, k the wave vector and ϕ_i are constant phases [5]. In the following I will always consider the (ξ, η)-plane at $\zeta = 0$.

Linear polarization Again considering a monochromatic, time invariant wave with angular frequency ω, the field vector $\vec{E}$ of a linearly polarized wave will be given [5] by

$$\vec{E} = \begin{pmatrix} A_\xi \cos(\omega t + \phi_0) \\ A_\eta \cos(\omega t + \phi_0) \end{pmatrix} .$$

Note that the phase angle ϕ_0 is the same for the ξ- and the η-component. The resulting motion and its projection onto the (ξ, η) plane are shown in Figure 2.1. It can clearly be seen that, for linearly polarized waves, the oscillation is always oriented in one specific direction (azimuth, θ), which depends only on the ratio between A_ξ and A_η, where

$$\theta = \arctan \frac{A_\eta}{A_\xi}$$

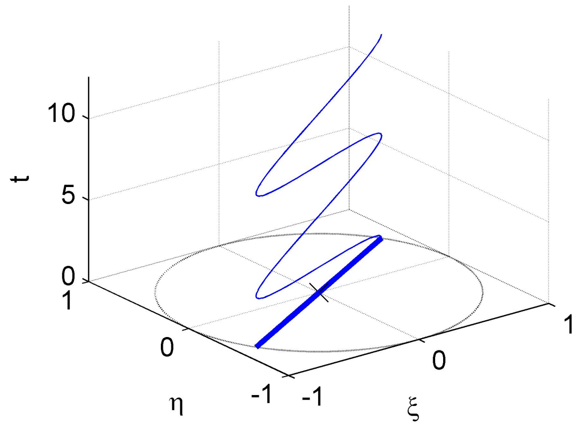

Figure 2.1.: Motion of a linearly polarized wave and its projection onto the (ξ, η)-plane.

Circular polarization Circular polarization refers to waves in which the oscillating quantity at a certain position in space has the same magnitude at all moments in time, but rotates cyclically in the plane orthogonal to the direction of propagation of the wave [5]. In this case we can write

$$\vec{E} = \begin{pmatrix} A_0 \cos(\omega t + \phi) \\ A_0 \cos(\omega t + \phi + \frac{\pi}{2}) \end{pmatrix}.$$

Note that the amplitude A_0 is the same for the ξ- and the η-component and that the two components have a phase difference of $\pi/2$. This results in $\left|\vec{E}\right| = \text{const} \quad \forall t$. The resulting vibrational motion and its projection onto the (ξ, η)-plane can be seen in Figure 2.2. For circular polarization we cannot define an azimuth angle.

Elliptical polarization As mentioned, elliptical polarization is the most general case of polarization. Every transverse, time-harmonic, monochromatic wave is elliptically polarized. The amplitude-vector at $\zeta = 0$ is given

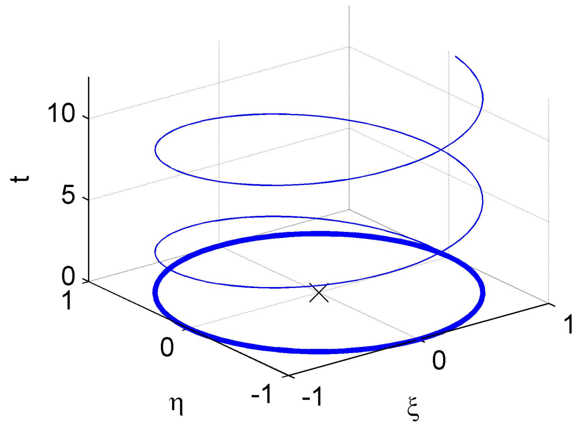

Figure 2.2.: Motion of a circularly polarized wave and its projection onto the (ξ, η)-plane.

[5] by

$$\vec{E} = \begin{pmatrix} A_\xi \cos(\omega t + \phi_\xi) \\ A_\eta \cos(\omega t + \phi_\eta) \end{pmatrix}. \tag{2.1}$$

This equation describes an ellipsis in the (ξ, η)-plane (see Figure 2.1.1). This

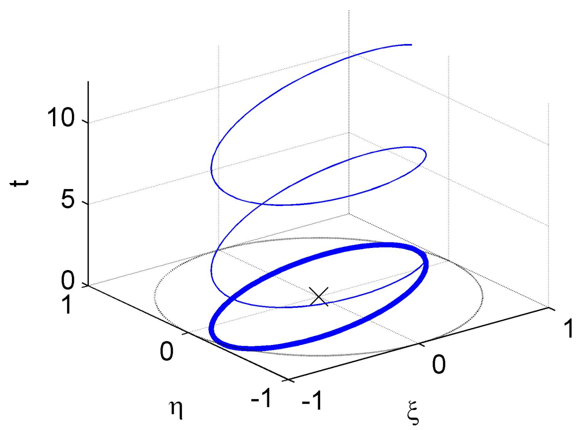

Figure 2.3.: Motion of an elliptically polarized wave and its projection onto the (ξ, η)-plane.

can be seen more easily [4] by rewriting Eq. (2.1) (see Appendix A.1) to give

$$\frac{E_\xi^2}{A_\xi^2} + \frac{E_\eta^2}{A_\eta^2} - 2\frac{E_\xi E_\eta}{A_\xi A_\eta} \cos(\phi_\eta - \phi_x i) = \sin^2(\phi_\eta - \phi_\xi),$$

or in matrix notation

$$\begin{pmatrix} E_\xi & E_\eta \end{pmatrix} \begin{pmatrix} A_\xi^2 & -A_\xi A_\eta \cos(\phi_\eta - \phi_\xi) \\ -A_\xi A_\eta \cos(\phi_\eta - \phi_\xi) & A_\eta^2 \end{pmatrix} \begin{pmatrix} E_\xi \\ E_\eta \end{pmatrix}$$
$$= A_\xi^2 A_\eta^2 \sin^2(\phi_\eta - \phi_\xi).$$

Both expressions represent elliptical equations. The latter can be rotated to the principal axis system. The rotation angle (azimuth) θ will thereby depend on A_ξ, A_η, ϕ_ξ and ϕ_η [4] and defines the direction of the semi-major axis. Note that for $\phi_\xi \neq \phi_\eta$ the azimuth θ will *not* be given by $\arctan A_\eta A_\xi$, but has a more complicated form.

The polarization state of a monochromatic wave is fully described by either the ratio of A_ξ to A_η and the magnitude and sign of the phase difference $\phi_\eta - \phi_\xi$ or the rotation angle θ, the ellipticity and handedness (i.e. the rotation direction). (Note that the semi-major axis and hence the azimuth is not well defined for circularly polarized waves.)

The Jones Vector

The Jones Vector J is a complex, two-row column vector [5], derived from the complex (analytic) form $\vec{E}^c$ of the field vector

$$\vec{E}^c = \begin{pmatrix} A_\xi e^{i(\omega t + \phi_\xi)} \\ A_\eta e^{i(\omega t + \phi_\eta)} \end{pmatrix} = e^{i\omega t} e^{i\phi_\xi} \begin{pmatrix} A_\xi \\ A_\eta e^{i\phi} \end{pmatrix}, = e^{i\omega t} A \begin{pmatrix} \cos(\chi) \\ \sin(\chi) e^{i\phi} \end{pmatrix};$$

$$J = \begin{pmatrix} \cos(\chi) \\ \sin(\chi) e^{i\phi} \end{pmatrix}, \tag{2.2}$$

where $\phi = \phi_\eta - \phi_\xi$, $A = \sqrt{A_\xi^2 + A_\eta^2} e^{i\phi_\xi}$ and $\chi = \arctan A_\eta / A_\xi$. This definition holds all polarization information given by Ey. 2.1, since the latter is simply given by the real part of the former.

Using this complex vector, there is another method to determine the azimuth and the ellipticity: Find the angle ψ that maximizes the sum of the squared real parts of $e^{-i\psi}\vec{E}^c$. The semi-major axis then corresponds to the real part of $e^{-i\psi}\vec{E}^c$, and the semi-minor axis to its imaginary part [6]. Azimuth and ellipticity can then be obtained from the vectors of the semi-major and semi-minor axes. The azimuth is thereby restricted to $[0; 180]^\circ$ to resolve the ambiguity shown in Fig. 2.4

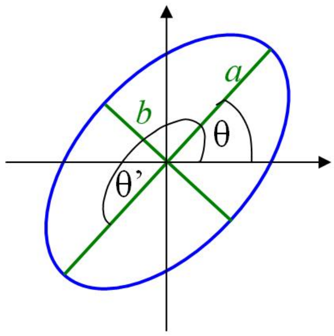

Figure 2.4.: Semi-major and semi-minor axis; the azimuth θ and its ambiguity.

2.1.2. Partial Polarization and the Coherency Matrix

Since every monochromatic wave can be expressed by Eq. (2.1), which in turn defines a specific polarization state, every monochromatic wave is inherently completely polarized. If, however, the amplitudes $A_\xi(t)$ and $A_\eta(t)$, and (or) the phases $\phi_\xi(t)$ and $\phi_\eta(t)$ are time dependent, the resulting wave is not necessarily completely polarized.. Time dependent amplitudes and phases authomatically involve a certain spectral bandwidth of the signal. The waves are then not not easily analyzed by their field vectors (or Jones vectors) [4]. In such cases, the concept of the coherency matrix C becomes important. The coherency matrix (or polarization matrix) as presented in the following is adequate for describing the coherence and the polarization phenomena of a narrow-band stochastic transverse wave [7]. Following e.g. Ref. [5] or [8], the coherency matrix (or polarization matrix, or, in seismic applications, correlation matrix) is given by

$$C = \begin{pmatrix} \left\langle E_\xi^{c*} E_\xi^c \right\rangle & \left\langle E_\eta^{c*} E_\xi^c \right\rangle \\ \left\langle E_\xi^{c*} E_\eta^c \right\rangle & \left\langle E_\eta^{c*} E_\eta^c \right\rangle \end{pmatrix}, \tag{2.3}$$

where $\langle\cdot\rangle$ denotes a time average, and the asterisks denote the complex conjugate. The degree of polarization [5, 4] is defined as

$$\mathcal{P} = \sqrt{\frac{1 - 4\det(C)}{\mathrm{tr}(C)^2}}. \tag{2.4}$$

Note that this definition is rotationally invariant, but the averaging time (i.e. the time window used when building the time average) can influence the resulting degree of polarization [5]

One can also introduce a spectral coherency matrix S [7] given by

$$S = \begin{pmatrix} \left\langle \tilde{E}_\xi^* \tilde{E}_\xi \right\rangle_\omega & \left\langle \tilde{E}_\eta^* \tilde{E}_\xi \right\rangle_\omega \\ \left\langle \tilde{E}_\xi^* \tilde{E}_\eta \right\rangle_\omega & \left\langle \tilde{E}_\eta^* \tilde{E}_\eta \right\rangle_\omega \end{pmatrix}, \tag{2.5}$$

where $\tilde{E}$ denotes the Fourier transform of E and $\langle\cdot\rangle$ denotes an average over all frequencies. For monochromatic waves the spectral coherency matrix is replaced by the coherency matrix as given above.

2.1.3. Polarization of Elastic Waves in Media

Elastic waves in liquids or gases can only have a longitudinal mode, as shear stresses are negligible in these media. For longitudinal waves, the vibrational motion (i.e. the direction of particle motion for elastic waves) is always parallel to the direction of propagation. Hence, longitudinal waves are usually said no to possess the property of polarization.

In solids, such as rocks, on the other hand, elastic waves can also have a transverse mode, and can therefore be polarized. Since, in the longitudinal mode, the direction of vibrational motion is constant, I will henceforth refer to the longitudinal mode as being linearly polarized in the direction of motion. This generalization of the concept of polarization, makes an extension of the formalism described in Section 2.1.1 necessary. Due to the longitudinal motion, we can no longer restrict the analysis to the two-dimensional (ξ, η)-plane perpendicular to the direction of motion. Instead we need to consider the motion in three dimensions. Hence, we write in analogy to Eq. (2.1) the full field vector as

$$\vec{E} = \begin{pmatrix} A_x \cos(\omega t + \phi_x) \\ A_y \cos(\omega t + \phi_y) \\ A_z \cos(\omega t + \phi_z) \end{pmatrix} . \tag{2.6}$$

This equation describes an ellipsis, which does not lie in a 2D space restricted by the direction of propagation of the wave, but in an arbitrary 2D plane in the 3D space. The orientation of the 2D plane thereby depends on the amplitudes $A_{\{x,y,z\}}$ and the phase angles $\phi_{\{x,y,z\}}$. In analogy to the complex Jones vector given in Eq. (2.2), we can also write down a complex (analytic), three-dimensional vector given by

$$\vec{E}^c = \begin{pmatrix} A_x e^{i(\omega t + \phi_x)} \\ A_y e^{i(\omega t + \phi_y)} \\ A_z e^{i(\omega t + \phi_z)} \end{pmatrix} . \tag{2.7}$$

The orientation of the ellipsis in space can be found, similarly to the two-dimensional case described in Section 2.1.1, either by a principal axis transformation or by maximizing the length of the real part of $e^{-i\psi}\vec{E}^c$, and taking $\Re(e^{-i\psi}\vec{E}^c)$ and $\Im(e^{-i\psi}\vec{E}^c)$ as semi-major and semi-minor axis, respectively [6].

The same procedure of adding a third dimension can also be used for the coherency matrix and the spectral coherency matrix:

$$C = \begin{pmatrix} \langle E_x^{c*} E_x^c \rangle & \langle E_y^{c*} E_x^c \rangle & \langle E_z^{c*} E_x^c \rangle \\ \langle E_x^{c*} E_y^c \rangle & \langle E_y^{c*} E_y^c \rangle & \langle E_z^{c*} E_y^c \rangle \\ \langle E_x^{c*} E_z^c \rangle & \langle E_y^{c*} E_z^c \rangle & \langle E_z^{c*} E_z^c \rangle \end{pmatrix}, \tag{2.8}$$

$$S = \begin{pmatrix} \left\langle \tilde{E}_x^* \tilde{E}_x \right\rangle_\omega & \left\langle \tilde{E}_y^* \tilde{E}_x \right\rangle_\omega & \left\langle \tilde{E}_z^* \tilde{E}_x \right\rangle_\omega \\ \left\langle \tilde{E}_x^* \tilde{E}_y \right\rangle_\omega & \left\langle \tilde{E}_y^* \tilde{E}_y \right\rangle_\omega & \left\langle \tilde{E}_z^* \tilde{E}_y \right\rangle_\omega \\ \left\langle \tilde{E}_x^* \tilde{E}_z \right\rangle_\omega & \left\langle \tilde{E}_y^* \tilde{E}_z \right\rangle_\omega & \left\langle \tilde{E}_z^* \tilde{E}_z \right\rangle_\omega \end{pmatrix}, \tag{2.9}$$

The degree of polarization can still be defined as

$$\mathcal{P} = \sqrt{\frac{1 - 4\det(C)}{\mathrm{tr}(C)^2}}.$$

2.1.4. The Analytic Signal and the Fourier Transform

In order to characterize the polarization of a signal using Eq. (2.1) or Eq. (2.6), we need to know the signal at more than one moment in time, even if we assume the signal to be completely monochromatic and time independent. Evaluating Eq. (2.1) or Eq. (2.6) at one moment in time gives one real vector with two (three) real entries. These two (three) values are not sufficient to determine the two (three) amplitudes *and* phases necessary to fully describe polarization. However, considering Eqs. (2.2) and (2.7) instead, we find that the knowledge of $\vec{E}^c$ at one moment in time is sufficient to completely characterize the polarization since both, the real and the imaginary part of the signal, can be used to determine the amplitudes and (relative) phases. Unfortunately, the complex form of the signal $\vec{E}$ is only a mathematical construct and cannot be measured in any physical measurement setup. However, knowing the complete time series $\vec{u}(t)$ of a signal (as given in Eqs. (2.1) and (2.6) for a monochromatic wave), the analytic signal $u^c(t)$ can be constructed by

$$u^c(t) = u(t) + i * \mathcal{H}(u(t)),$$

where $\mathcal{H}$ denotes the Hilbert transform. Indeed, the so constructed analytic signal of the $\cos(\omega t+\phi)$-term in Eqs. (2.1) and (2.6) is given by $\exp(i(\omega t+\phi))$, for $\omega > 0$, which is exactly the expression used in the Jones vectors Eqs. (2.2) and (2.7). Hence, the analytic signal can be used to infer the polarization of a wave at each instant in time. Although the polarization can such be calculated at each moment in time, the signal is still only considered to be polarized, if the polarization characteristics stays stable over a certain time window larger than the oscillation period of the signal [9].

In order to understand the meaning of the analytic signal, it is very instructive to take a closer look at the properties of the analytic signal in connection with the Fourier transform: The Hilbert transform's Fourier transform of a signal is always rotated by $-i$ or i in the complex plane for positive and negative frequencies, respectively, when compared to the Fourier transform of the signal itself. The analytic signal is hence composed by the signal plus i times the phase rotated signal. This implies that the Fourier transform of the analytic signal of a real time series is twice the Fourier transform of the real time series for positive frequencies and is zero otherwise.[1] This discussion also makes clear that, due to the composition of the analytic signal from signal plus phase shifted signal, the analytic signal at each instant in time "knows" something of the signal at other times. This follows also from the definition of the Hilbert transform, which involves an integral over all times.

Similarly, the Fourier transform requires the knowledge of the signal at all moments in time, since it is based on a weighted time integral of the signal.

[1] Consider for example the time series $u(t) = \cos(\omega_0 t)$. The Hilbert transform of u is given by $\mathcal{H}(u(t)) = \sin(\omega_0 t) = \cos(\omega_0 t - 90)$. The Fourier transform of u is given by $\mathcal{F}(u(t)) = 1/2\,[\delta(\omega - \omega_0) + \delta(\omega + \omega_0)]$. Shifting the first term in the bracket, corresponding to positive frequencies by $-i = 1/i$, and the second term by $i = -1/i$ gives $1/(2i)\,[\delta(\omega - \omega_0) - \delta(\omega + \omega_0)]$, which is the Fourier transform of $\sin(\omega_0 t)$ and hence $\mathcal{F}\,[\mathcal{H}(u(t))]$. Combining these results gives $\mathcal{F}\,[u(t) + i\mathcal{H}(u(t))] = \delta(\omega - \omega_0)$, which is twice the positive frequency part of $\mathcal{F}(u(t))$.

Hence, knowing the Fourier transform, we expect to have all information necessary to perform a polarization analysis (which involves, as noted, the knowledge of the signal at several moments in time). That this is indeed true becomes obvious when looking at at the inverse Fourier transform

$$\vec{u}(t) = \int_{-\infty}^{\infty} e^{2\pi ft} \vec{U}(f) \mathrm{d}f, \tag{2.10}$$

where $\vec{U}(f)$ is the Fourier transform of $\vec{u}(t)$. Since $\vec{U}(f)$ is a complex quantity, we can rewrite U as $U_\alpha(f) = E_\alpha e^{i\phi_\alpha}$, where $\alpha = \{x, y, z\}$. Setting $\omega = 2\pi f$, we find that Eq. (2.10) is only a generalization of Eq. (2.7) for a superposition of several frequencies. Hence, the complex valued Fourier transform $\vec{U}(f)$ of a signal completely characterizes the polarization of each frequency component of a wave, in the same way as the polarization is characterized by the Jones vector or analytic signal.

2.1.5. Eigenvalue Decomposition of the coherency matrix

In order to analyze the polarization of time-dependent signals in time-domain, it is useful to consider the signal's covariance matrix. In many geophysical applications it is furthermore a common procedure to perform an eigenvalue decomposition thereof, or, equivalently a singular value decomposition of the signal itself [4, 10]. In order to understand the mechanisms involved in the polarizations analysis of seismic waves described in the next chapter, it is necessary to understand in depth what such a decomposition applied to seismic signals can elucidate.

To this end, consider a three component time-series given by the vectors $\vec{X}$, $\vec{Y}$ and $\vec{Z}$, where each entry corresponds to one discrete time-step. These time-series can be combined into a $n \times 3$ signal matrix

$$D = [XYZ]. \tag{2.11}$$

Performing a singular value decomposition (SVD) of the matrix D, we obtain the following decomposition $D = U\Sigma V^T$, where U and V are orthogonal $n \times n$ and 3×3 matrices respectively, and Σ is a generalized diagonal matrix of dimension $n \times 3$ containing the singular values $\sigma_1 \geq \sigma_2 \geq \sigma_3 \geq 0$ [11]. Consider now the simple case for which $\sigma_2 = \sigma_3 = 0$. Writing $U = [\vec{u}_1 \vec{u}_n \ldots \vec{u}_n]$ and $V = [\vec{v}_1 \vec{v}_2 \vec{v}_3]$ leads to the following expression for D

$$D = \left(\begin{pmatrix} \vdots \\ \vdots \\ \vec{u}_1 \\ \vdots \\ \vdots \end{pmatrix} \begin{pmatrix} \vdots \\ \vdots \\ \vec{u}_2 \\ \vdots \\ \vdots \end{pmatrix} \cdots \begin{pmatrix} \vdots \\ \vdots \\ \vec{u}_n \\ \vdots \\ \vdots \end{pmatrix} \right) \begin{pmatrix} \sigma_1 & & \\ & 0 & \\ & & 0 \\ & \vdots & \\ \cdots & 0 & \cdots \\ & \vdots & \end{pmatrix} \begin{pmatrix} \begin{pmatrix} \cdots & \vec{v}_1^T & \cdots \end{pmatrix} \\ \begin{pmatrix} \cdots & \vec{v}_2^T & \cdots \end{pmatrix} \\ \begin{pmatrix} \cdots & \vec{v}_3^T & \cdots \end{pmatrix} \end{pmatrix}$$

$$D = \sigma_1 \begin{pmatrix} u_{1,1}v_{1,1} & u_{1,1}v_{1,2} & u_{1,1}v_{1,3} \\ u_{1,2}v_{1,1} & u_{1,2}v_{1,2} & u_{1,2}v_{1,3} \\ \vdots & \vdots & \vdots \\ u_{1,n}v_{1,1} & u_{1,n}v_{1,2} & u_{1,n}v_{1,3} \end{pmatrix},$$

where $u_{i,j}$ and $v_{i,j}$ denote the j-th component of the vectors $\vec{u}_i$ and $\vec{v}_i$ respectively. Thus, the signal matrix D is simply composed of σ_1 times the time series $\vec{u}_1$ projected into the direction of $\vec{v}_1$. The resulting signal therefore describes a perfectly linear motion in the direction of $\vec{v}_1$. However, the signal is not necessarily coherent and could, for example, also result from random noise with one component only.

In the general case, where $\sigma_1 \geq \sigma_2 \geq \sigma_3 \geq 0$, the seismic data D is composed of the sum of $\sigma_1\vec{u}_1$ projected in $\vec{v}_1$-direction, $\sigma_2\vec{u}_2$ projected in $\vec{v}_2$-direction and $\sigma_3\vec{u}_3$ projected in $\vec{v}_3$-direction. Since the $\vec{u}_i$ form an orthonormal system, the portion of the data being linear in direction $\vec{v}_i$, is given by the relative size of σ_i compared to the two other singular values. If $\sigma_1 \gg \sigma_2 \geq \sigma_3$, then the motion is predominantly linear. If, however, $\sigma_1 \simeq \sigma_2 \gg \sigma_3$, the motion is mostly confined to a plane spanned by $\vec{v}_1$ and $\vec{v}_2$.

Alternatively, we can compute the signal's coherency matrix M

$$M = D^T D. \tag{2.12}$$

(Note that the signal's covariance matrix is similar to the coherency matrix. The only difference is that in the calculation of the coherency matrix the analytic signal $D^C = [X^c, Y^c, Z^c]$ is used instead of the signal $D = [X, Y, Z]$ itself.) Calculating the singular value decomposition of D is equivalent to performing the eigenvalue decomposition of the signal's covariance matrix

M, since

$$M = D^T D = (U\Sigma V^T)^T (U\Sigma V^T) = V\Sigma^2 V^T = \sum_{i=1}^{3} \sigma_i^2 \vec{v}_i \vec{v}_i^T$$
$$M = \sum_{i=1}^{3} \lambda_i \vec{\Lambda}_i \vec{\Lambda}_i^T,$$

The eigenvectors $\vec{\Lambda}_i$ of M thus correspond to the right singular vectors $\vec{v}_i$ of the signal matrix D ($\vec{\Lambda}_i = \vec{v}_i$), and the eigenvalues λ_i correspond to the square of the singular values σ_i^2 ($\lambda_i = \sigma_i^2$). Hence, the eigenvector corresponding to the greatest eigenvalue describes the main direction of motion as the first right singular vector did in the case of the singular value decomposition.

Since the covariance matrix M is symmetric and positive semi-definite, the eigenvalues and eigenvectors of M can also be found by performing a singular value decomposition. In this case, the right singular vectors will be the same as the left singular vectors of M and will be equal to the eigenvectors of M; the singular values of M correspond to the eigenvalues of M. Using the SVD instead of the eigenvalue decomposition might be desirable in computational applications, as in the SVD, the singular values are, per definition, given in decreasing order.

Time Dependent Polarization Using the Analytic Signal

If we had used the analytic counterparts $\vec{X}^c$, $\vec{Y}^c$, and $\vec{Z}^c$ instead of $\vec{X}$, $\vec{Y}$, and $\vec{Z}$ to construct D^c and $M^c = C$, the vectors $\vec{u}_i$ and $\vec{v}_i$ would be complex. In the last section, I explained how the vector $\vec{v}_i$ describes a linear direction of motion. In the analytic case, the vectors $\vec{v}_i$ do not describe linear motion, but a motion on an ellipsis (The vector $\vec{v}_i$ can be interpreted as Jones vector (See Section 2.1.1) and can hence be interpreted in the same way as the Jones vector as an ellipsis).

3. Polarization Analysis of Seismic Waves

In the past, several different methods for the polarization analysis of seismic waves and subsequent polarization filtering have been devised. Many of these rely on the coherency matrix or the spectral coherency matrix (e.g. [1, 12, 13, 14, 10, 15, 16]; some of these are reviewed in [17]). Others simply analyze the Jones vector at each instant in time (e.g. [9, 6] and [18]). Another type of methods uses transformations aiming at optimal time-frequency resolution such as the wavelet transform (not discussed here) or the less well known S-transform (e.g. [19]). Due to their similarity, I will combine all methods relying on the signal's covariance matrix, the analytic signal's covariance matrix, and the spectral coherency matrix under the header"coherency matrix methods".

3.1. Coherency Matrix Methods

3.1.1. CovarianceMatrixMethods

This method goes back to the 1970's and was first suggested in this form by Flinn [1]. The method is based on the theory discussed in Section 2.1.2, but uses the signal itself instead of the analytic signal and makes use of the considerations in Section 2.1.5. The procedure is the following

1. Build the signal's covariance matrix M over a given time window

$$M = \begin{pmatrix} X^TX & X^TY & X^TZ \\ Y^TX & Y^TY & Y^TZ \\ Z^TS & Z^TY & Z^TZ \end{pmatrix},$$

   where X, Y, Z are column vectors containing the signal's x, y and z component over a certain time window, possibly a tapered time window with center time t.

2. Move the time window along the trace data to obtain a discrete function $M(t)$.

3. Perform an eigenvalue decomposition as suggested in Section 2.1.5 to obtain the eigenvalues $\lambda_i(t)$, and the eigenvectors $\vec{\Lambda}_i(t)$.

4. Calculate the polarization attributes as outlined below.

Linearity Flinn suggested a measure of linearity given by

$$L = 1 - \lambda_2/\lambda_1, \tag{3.1}$$

where λ_1 and λ_2 are the largest and intermediate eigenvalues of the signal's covariance matrix M defined by Eqs. (2.11) and (2.12). In Flinn's original paper and in many subsequent papers, L is called "rectilinearity". I will not use this term in order to avoid confusion with the usual definition of rectilinearity, which means that the wavefront is always perpendicular to the ray trace. The linearity L is near to 1 only if the direction of motion is strongly confined to one direction given by the eigenvector corresponding to λ_1.

The definition of linearity given in Eq. (3.1) is equivalent to that given later by Hearn [17]. Kennett [18], however, suggested a differing definition given by

$$\tilde{L} = 1 - \frac{\lambda_2 + \lambda_3}{2\lambda_1},$$

where λ_1 to λ_3 refer to the eigenvalues of M in decreasing order. The two definitions are very similar, but $\tilde{L}$ will decrease more slowly than L, if $\lambda_2 \gg \lambda_3$, i.e. if the signal is confined to a plane. This is why I will use Flinn's definition of linearity given in Eq. (3.1) in the code.

At this point, I would like to compare the measure of linearity L and $\tilde{L}$ with the measure of the degree of polarization given in Eq. (2.4). When exchanging C with M, the degree of polarization $\mathcal{P}$, according to Eq. (2.4) is given by

$$\mathcal{P} = \sqrt{1 - \frac{4\lambda_1\lambda_2\lambda_3}{(\lambda_1 + \lambda_2 + \lambda_3)^2}}.$$

For $\lambda 1 \gg \lambda 2 \gg \lambda 3$ this expression simplifies to

$$\mathcal{P} \approx 1 - \frac{2 * \lambda_2}{\lambda_1},$$

which is a very similar expression to (3.1). Although $\mathcal{P}$ would be a suitable measure of linearity, the approximation of $\mathcal{P}$ is not, since it is not bounded by $[0, 1]$. Figure 3.1 shows a comparison of L and P for the two dimensional case.

Planarity Kennett [18] also suggested a measure of planarity given by

$$P = 1 - \frac{2\lambda_3}{\lambda_1 + \lambda_2}. \tag{3.2}$$

The measure of planarity P will be approximately one if $\lambda_3 \ll \lambda_2 + \lambda_1$, i.e. if the direction of motion is confined to a plane spanned by the eigenvectors corresponding to the two larger eigenvalues λ_1 and λ_2. However, if the signals motion is highly linear and hence $\lambda_1 \gg \lambda_3$, the planarity is also near to one, since the linear motion is naturally also confined to a plane. This means that

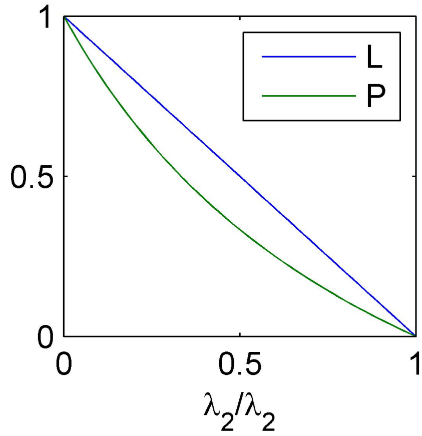

Figure 3.1.: Comparison: Degree of linearity as given by Eq. (3.1) and the degree of polarization given by Eq. (2.4)

the motion is only strongly elliptical or circular if $P \rightarrow 1$ and $L \rightarrow 0.5$

Apparent Azimuth If the signals linearity L is high, the apparent azimuth [18, 17] can be defined as

$$\theta = \arctan\left(\frac{\Lambda_{1,E}}{\Lambda_{1,N}}\right), \tag{3.3}$$

where $\Lambda_{1,E}$ and $\Lambda_{1,N}$ denote the east and north component of the eigenvector $\vec{\Lambda}_1$ corresponding to the largest eigenvalue of M. The use of a simple arctan-function as implemented in standard mathematic software and as also used in common calculators is sufficient due to the fundamental ambiguity of the polarization vector mentioned in Section 2.1.1. Since the apparent azimuth only specifies the direction of the dominant signal direction [18], the apparent azimuth will be less meaningful, the lower the signals linearity L is.

Apparent Incidence As for the apparent azimuth, high linearity is required in order to obtain an informative value for the apparent incidence. The apparent angle of incidence [18] (measured from the Z-direction) is given by

$$\alpha = \arccos(\Lambda_{1,Z}), \tag{3.4}$$

where $\Lambda_{1,Z}$ is the Z-component of the *normalized* eigenvector corresponding to the largest eigenvector of M.

This definition is equivalent to the definition given by Hearn [17]

$$d = \arctan\left(\frac{\Lambda_{1,Z}}{\sqrt{\Lambda_{1,E}^2 + \Lambda_{1,N}^2}}\right),$$

where d is the dip-angle measured for the horizontal correlated to the incidence angle by $d = 90 - \alpha$.

Implementation

I implemented this method in SEISMON using a Tukey window with a ratio of 0.1 of the cosine taper to the constant section. The length of the window is adjustable. The calculated polarization attributes are the degree of linearity L, given by equation (3.1) and the planarity P given by equation (3.2). Furthermore the azimuth Eq. (3.3) and the incidence angle Eq. (3.4) are outputted. For instruction manuals refer to Appendix B. Additionally, one can optionally display an angle between the eigenvector corresponding to the largest eigenvector at specified time-window and all other time windows (see Appendix B for information on how to access this tool).

3.1.2. Debiased Covariance Matrix Method

This method is identical to the Covariance Matrix Method, except for the fact that in the Debiased Covariance Matrix Method the mean of each windowed time-series is subtracted from the windowed values. This might be an advantage if there is very low frequency noise contained in the data. This problem can be circumvented, though, by applying a high pass filter to the data before analyzing it.

Implementation

The implementation and the outputted attributes are the same as for the Covariance Matrix Method (see Section 3.1.1).

3.1.3. Complex Covariance Matrix Method

This method was introduced by Vidale in 1986 [13] and is based on the complex covariance matrix (or coherency matrix) $M^c = C = (D^c)^T D^c$, where $D^c = [X^c Y^c Z^c]$ is composed of the analytic signals of the column vectors containing the data of the seismic traces X, Y and Z. This method is thus equivalent to the standard procedure used in optics for the polarization analysis of narrow-band signals (see Section (2.5)). However, Vidale extended this theory insofar as he suggested to perform an eigenvalue decomposition of the coherency matrix (as already done in the previous two methods). As mentioned in Section 2.1.5, this leads to complex polarization vectors, which describe a polarization ellipsis and not linear polarization. The complex eigenvector Λ_1^c corresponding to the largest eigenvalue, describes again the signal's predominant motion. Summing up, the complex covariance matrix method differs from the covariance matrix method only in the fact that the former uses the analytic signal and the latter the signal itself.

As explained in Section 2.1.1, the semi-major and semi-minor axis of the ellipsis described by the complex vector $\vec{\Lambda}_1^c$ can be found by several means. Vidale proposes to rotate the eigenvector in the complex plane, such that the real component of the rotated vector is maximized. This method was already mentioned in connection with Eq. (2.7). Since this method is unstable if the signal is circularly polarized, I used a slightly altered maximization procedure proposed by Morozov and Smithson [6]. They proposed to find the semi-major and semi-minor axes of a complex vector $\vec{\Lambda}_1^{\,c}$ by maximizing

$$\sum_i \left[\Re\left(e^{-i\psi}\Lambda^c_{1,i}\right)\right]^2 + \varepsilon\left[\sum_i \Re\left(e^{-i\psi}\Lambda^c_{1,i}\right)\right]^2,$$

with respect to ψ. The value $\varepsilon \ll 1$ is the regularization parameter, $\Re$ denotes the real part.

Morozov and Smithson also give an analytic expression for the rotation angle ψ

$$\psi = \frac{1}{2}\arg\left[\frac{1}{2}\sum_i(\Lambda^c_{1,i})^2 + \varepsilon\frac{1}{2}\left(\sum_i \Lambda^c_{1,i}\right)^2\right]. \tag{3.5}$$

With this angle ψ, the semi-major axis $\vec{a}$ and semi-minor axis $\vec{b}$ is then given by

$$\vec{a} = \Re\left[e^{-i\psi}\vec{\Lambda}^c_1\right] \tag{3.6}$$

$$\vec{b} = \Im\left[e^{-i\psi}\vec{\Lambda}^c_1\right]. \tag{3.7}$$

Degree of Polarization Vidale [13] proposed a measure for the degree of polarization defined by

$$\tilde{L}^c = 1 - \frac{\lambda^c_2 + \lambda^c_3}{\lambda^c_1},$$

where λ^c_1 to λ^c_3 denote the eigenvalues of the complex covariance matrix M^c in decreasing order. This choice seems unfortunate since it is not bounded by $[0,1]$, as becomes obvious when considering the case of the unit matrix. In this case $\lambda^c_1 = \lambda^c_2 = \lambda^c_3 = 1$ and hence $\tilde{L} = -1$. In analogy to the measure of linearity used in case of the real valued covariance matrix, I will rather use

$$L^c = 1 - \lambda^c_2/\lambda^c_1, \tag{3.8}$$

where λ_1^c and λ_2^c are the largest and intermediate eigenvalues of the signal's complex covariance matrix M^c. In spite of the analogy of L^c to L, as defined in Eq. (3.1), it is of utmost importance to keep in mind that L^c does *not* give a measure of linearity! Since Λ_1^c describes an ellipsis, L^c will not only be near to one, if the motion is strongly linear, but also if it is strongly elliptical.

Ellipticity A measure of the motion's linearity can be obtained from the inverse ellipticity, i.e. the ratio of the semi-minor axis to the semi-major axis. (A quantity dubbed "elliptical component of polarization" by Vidale in [13].)

$$e^c = \frac{\left|\vec{b}\right|}{|\vec{a}|}. \tag{3.9}$$

This quantity is one for perfectly circular motion and zero for perfectly linear motion, and will be only meaningful, if L^c is high.

Apparent Azimuth The apparent azimuth can be calculated by

$$\theta^c = \arctan\left(\frac{a_E}{a_N}\right), \tag{3.10}$$

where a_E and a_N are the east and north component of the semi-major axis, respectively. The apparent azimuth angle is only meaningful, if L^c is high and e^c is low.

Apparent Incidence The apparent incidence angle is given by

$$\alpha = \arccos\left(\frac{a_Z}{|\vec{a}|}\right), \tag{3.11}$$

where a_Z is the vertical component of the semi-major axis a.

Implementation

I implemented this method using a sliding Tukey window as in the two previous methods. The semi-major and semi-minor axes of the ellipsis described by the eigenvector corresponding to the largest eigenvalue was calculated using the equations stated above. The calculated attributes are the degree of polarization Eq. (3.8), the ellipticity of the eigenvector corresponding to the largest eigenvalue Eq. (3.9) and azimuth and incidence angle (Eqs. (3.10) and (3.11)).

3.1.4. Spectral Matrix Method

Instead of analyzing the covariance matrix of the time series of the three component seismic signal, the signal can also be analyzed in frequency domain, by calculating the covariance matrix S of the signals Fourier transforms $\tilde{X}(f)$, $\tilde{Y}(f)$ and $\tilde{Z}(f)$ (See Section 2.1.2). This approach was suggested for the analysis of seismic data by Samson and Olson in 1981 [15]. The procedure suggested in their paper [15] is the following:

1. If the time series is very long, use a sliding window in time to obtain time segments of the tree component seismic data.

2. Perform a Fourier transform of each time segment. (The first and second point can be combined by performing a short time Fourier transform.)

3. Build spectral matrices $S_i(\omega_{\text{mean}}, t_{\text{segment}})$, where the average $\langle\cdot\rangle_\omega$ (see Eq. (2.5)) is only taken over a spectral band $[\omega_i - \delta, \omega_i + \delta]$ for each time segment. The window width 2δ may be chosen rather short. Samson and Olson [15] suggest a window containing 5-6 discrete frequencies in order to retain a good estimate of the degree of polarization L^f (see next paragraph).

4. Calculate the Degree of Polarization for each of spectral matrix (see Eq. (3.12)).

The procedure outlined above allows for a certain resolution in time *and* frequency. Note, however, that the two resolutions rival each other: Very short time windows will lead to broadly spread discrete frequencies and hence low frequency resolution; high frequency resolution requires long time segments.

When performing an eigenvalue decomposition of the spectral matrices, one obtains frequency dependent eigenvalues and eigenvectors $\lambda_i^f(f)$ and $\vec{\Lambda}_i^f(f)$ instead of time-dependent quantities $\lambda_i(t)$ and $\Lambda_i(t)$. Due to the time-windowing, quantities λ_i^f and $\vec{\Lambda}_i^f$ actually depend on both, frequency *and* time. However, the former dependency is the distinguishing feature of the spectral matrix and the time resolution will hence usually be secondary. As in the time dependent case, I will suppress the explicit frequency (and time) dependency of λ_i^f and $\vec{\Lambda}_i^f$ and all derived quantities in the following.

Degree of Polarization Samson and Olson suggested the following measure of the degree of polarization for three-component seismograms

$$\tilde{L^f} = \frac{3\,\mathrm{tr}(S^2) - (\mathrm{tr}(S))^2}{2(\mathrm{tr}(S))^2}. \tag{3.12}$$

Since the trace of a matrix is invariant under rotations, and since S is hermitian, $\mathrm{tr}(S) = \sum_i \lambda_i^f$ and $\mathrm{tr}(S^2) = \sum_i (\lambda^f)^2$, where λ_i^f are the eigenvalues of S. Assuming $\lambda_1^f \gg \lambda_2^f \gg \lambda_3^f$, this definition for the degree of polarization goes towards

$$L^f = 1 - \frac{\lambda_2^f}{\lambda_1^f}, \tag{3.13}$$

where λ_1^f and λ_2^f are the largest and intermediate eigenvalues of S, respectively. I found that $\tilde{L^f}$ shows a stronger variation than L^f when applied to the data of local earthquakes. However, the second definition allows better comparability to the other methods (See Eqs. (3.1) and (3.8)).

Polarization Attributes Samson and Olson [15] do not use the eigenvectors Λ_i^f obtained from the eigenvalue decomposition to calculate polarization attributes. Instead they use the degree of polarization to devise a polarization filter. Nevertheless, according to the discussion in Section 2.1.4, obtaining polarization attributes from the eigenvalue decomposition of the spectral matrix S shoule be possible: The semi-major and semi-minor axes are found using Eqs. (3.5) to (3.6), when replacing Λ_i^c by Λ_i^f. Similarly to the complex covariance matrix method, the spectral matrix method can such be used to obtain the main polarizations attributes over a certain frequency band.

Implementation

I implemented this method in SEISMON using adaptable sliding windows in time and frequency, where the time overlap of the time windows is set to zero and the frequency overlap of the frequency window is user defined. The degree of polarization is calculated using Eq. (3.12) and (3.13), and are referred to as L and L^* respectively. The polarization attributes calculated are, as in the previous cases azimuth and incidence angle.

3.2. Instantaneous Attributes Method

Using the analytic signal, the vectors of the semi-major and semi-minor axes can be found at every instant in time by replacing Λ_i^f by $[X^c Y^c Z^c]$ in Eqs. (3.5) to (3.6). This method was suggested by Schimmel and Gallart [9].

Degree of Polarization The method outlined above, does not itself allow for an estimation of the degree of polarization (which is usually determined form a coherency matrix), since the analytic signal at a specific moment in time is always described by one specific ellipsis and is hence completely polarized. Schimmel and Gallart [9], however, introduced a measure of polarization. According to the named authors, polarization should be a feature of a signal that does not change during a certain time ΔT. We are hence in need of some measure that evaluates the change in polarization over ΔT in order to obtain a measure of the polarization. Note that in the complex covariance matrix method this measure was obtained by using a finite window length for the covariance matrix and comparing the size of the eigenvalues corresponding to orthogonal polarization states (i.e. the eigenvectors). Schimmel and Gallart suggest the following measure of polarization

$$L^i = \left[\left\langle (\hat{m} \cdot \hat{a}(\tau)^4 \right\rangle_{[t-\frac{\Delta T}{2}, t+\frac{\Delta T}{2}]} \right]^4 , \tag{3.14}$$

where $\hat{a}(\tau)$ is the normalized vector of the semi-major axis at time τ, and $\langle \ldots \rangle_{[t-\frac{\Delta T}{2}, t+\frac{\Delta T}{2}]}$ denotes the average taken over $\tau \in [t - \frac{\Delta T}{2}, t + \frac{\Delta T}{2}]$. The exponents may be adapted in order to achieve a proper dynamic in L^i. The normalized vector $\hat{m}$ can be defined as follows

$$\vec{m}_1 = \langle \vec{a} \rangle_{[t-\frac{\Delta T}{2}, t+\frac{\Delta T}{2}]} \qquad \text{or} \tag{3.15}$$

$$\vec{m}_2 = \langle \hat{a} \rangle_{[t-\frac{\Delta T}{2}, t+\frac{\Delta T}{2}]} , \tag{3.16}$$

where $\hat{a}$ is the semi-major axis. The second definition is suggested to attenuate strong bias caused by large-amplitude noise. This definition seems to be very similar to the procedure of building a covariance matrix.

The polarization attributes can be derived from the complex signal as explained in 2.1 (and as outlined in Ref. [6]),as already used in 3.1.3.

Ellipticity The Ellipticity is again given by

$$e^i = \frac{\left|\vec{b}\right|}{|\vec{a}|}, \tag{3.17}$$

where $\vec{a}$ and $\vec{b}$ denote the semi-major and semi-minor axes, respectively. This quantity is one for perfectly circular motion and zero for perfectly linear motion.

Apparent Azimuth The apparent azimuth can be calculated

$$\theta^i = \arctan\left(\frac{a_E}{a_N}\right), \tag{3.18}$$

where a_E and a_N are the east and north component of the semi-major axis of the ellipsis defined by $[X^c Y^c Z^c]$, respectively. The apparent azimuth angle is only meaningful, if e^i is low.

Apparent Incidence The apparent incidence angle is given by

$$\alpha = \arccos\left(\frac{a_Z}{|\vec{a}|}\right), \tag{3.19}$$

where a_Z is the vertical component of the semi-major axis a of the ellipsis defined by $[X^c Y^c Z^c]$.

Implementation

I implemented this method in Seismon. The degree of polarization is calculated using Eq. (3.14) with Eqs. (3.15) and (3.16) and referred to as 1 and 2, respectively. As polarization attributes the azimuth and incidence angles are returned.

3.3. S-Transform Method

The Stockwell-transform (or S-transform) was introduced by Stockwell et al. [20] and used by Pinnegar [19] to allow time-frequency dependent polarization filtering. In principle, the S-transform is similar to a short time Fourier transform, with the additional, important trait that the window function is explicitly frequency dependent: the window function at each frequency f is given by a Gaussian whose standard deviation is proportional to $T = 1/f$. Performing this transform on a signal $X(t)$, one can obtain, for each moment in time and frequency, the S-transform, denoted by $\tilde{X}^S(t, f)$. The time resolution of $\tilde{X}^S(t, f)$ relative to the signals frequency component f will thereby stay constant. Looking at the absolute time resolution, the time resolution will be low at low frequencies, since in this case the Gaussian is very broad; the absolute frequency resolution, on the other hand, will be good. The opposite is true at high frequencies, where the Gaussian approaches a delta-function.

Since the quantities $\tilde{X}^S$, $\tilde{Y}^S$ and $\tilde{Z}^S$ are, in general, complex and related to the Fourier transform, the S-transformed signals can be directly used to obtain time and frequency resolved polarization quantities (see Section 2.1.4) by replacing Λ_i^c with $[\tilde{X}^S \tilde{Y}^S \tilde{Z}^S]$ in Eqs. (3.5) to (3.6) (This is very similar to the approach used for the spectral matrix method). Similarly to the instantaneous attributes method, this method does not directly lead to a degree of polarization and no measure of polarization was introduced for this method. Fortunately, the human eye is extremely apt to find patterns in figures. We can use this ability to obtain a subjective degree of polarization simply from looking at the plots of the polarization attributes and looking for patterns (see Chapter 4).

Pinnegar used the length of the semi-major and semi-minor axis, the inclinations of the ellipse to the horizontal, the azimuth of the ascending node and the pitch of the semi-major axis to completely describe the polarization parameters. These parameters are the parameters typically used to describe the motion of a planet and correspond to the Eulerian angles used to rotate an ellipsis from the x-y plane to an arbitrary position (see Fig. 3.3). They are especially suited to describe signals which are not linearly polarized.

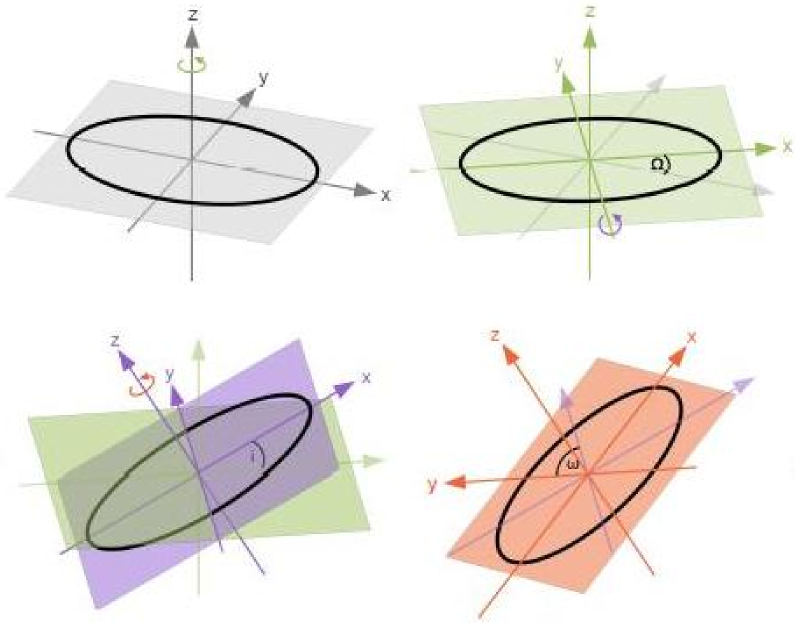

Figure 3.2.: Euler angles in y-convention used to describe an ellipsis in an arbitrary position. (Ω: azimuth of ascending node, ι: inclination of ellipsis plane, ω: pitch of semi-major axis.)

In order to allow comparison to the other methods and to allow easier interpretation of linear signals, I used the inverse ellipticity, and additionally to the "planetary parameters", the apparent azimuth and the apparent incidence angle as descriptive parameters. These parameters can be calculated by the same equations as given in Sections 3.2 or 3.1.3, and will not be repeated here.

Implementation

I implemented this methods to return the above named polarization attributes. In order to aid by identifying the signal containing regions in the time-frequency plots, the color is shaded with decreasing S-Transform amplitude.

3.4. Short Time Fourier Transform Method

The S-Transform method has one significant flaw: It is computationally sumptuous and easily exceeds Matlab's memory. I hence also implemented a similar method, this time using a short time Fourier transform (STFT) with sliding windows instead of the S-Transform. This, however, has the significant disadvantage, that the STFT does not adapt to the frequencies studied and is hence only optimal within a certain frequency band, which depends on the length of the time window used in the STFT.

3.5. Wavelet Transform Methods

For the sake of completeness, it has to be mentioned that some modern methods devised for the polarization analysis of seismic signals use a wavelet transform instead of an S-transform or a STFT. However, no such method was implemented in the course of this work ant will hence not be discussed in any mored detail here.

4. Global and Regional Earthquakes; Test and Discussion of Methods

4.1. Global Earthquakes; Discussion of Methods

4.1.1. Dataset

In order to test the different methods and to probe their abilities, I first applied the methods to global earthquake data. The reason that I chose to test the implemented methods on global earthquake data is that polarization analysis should work better with such data, since the different phases split up more strongly than in regional earthquakes and hence should follow their theoretical motion more exactly.

I investigated several global earthquakes; the analysis worked well with all methods, showing all expected features. As representative example, which will be presented here, I chose an event near the Nicobar islands (India region) with a magnitude of 7.7, which occurred in a depth of 35km [21]. The distance from this event's epicenter to the Austrian stations is $\Delta \approx 75°$. The data was taken from one of the broad-band seismometers maintained by the

Zentralanstalt für Meteorologie und Geophysik, Austria, namely from the Conrad observatory in Lower Austria.

Prior to the analysis the data was processed by removing the mean and by rotating the data in the horizontal plane into a coordinate system orientated relative to the event such that we obtain transverse and radial motion.

4.1.2. Discussion

Figure 4.1 shows the result of a polarization analysis of the afore described global earthquake using the covariance matrix method. The length of the time window was chosen to be 100s. Such a long averaging time is necessary due to the low frequency signal present. The effect of a too short averaging window will be discussed in detail later on (see Sec. 4.3).

In Figure 4.1 the linearity increases rapidly as soon as the (relatively high frequency and high amplitude) first arrival at $t \approx 200s$ enters the averaging window. This is somewhat expected since the first arrival should correspond to a P-wave which should be linearly polarized in the direction of the ray path. During the arrival of the P-wave coda, the linearity decreases continually. This in not surprising either since the successive arrival of different phases should decrease the linearity. The linearity increases once more at the first arrival of the S-wave (at $t \approx 750s$). The arriving S-waves has a much higher amplitude than the late P-wave arrivals and hence dominates in the polarization analysis leading to high linearity. The sudden decrease at in linearity $t \approx 1000s$ might be due to the arrival of the ScS-wave arriving shortly after the direct S-wave. At $t \approx 1120s$ the linearity increases once more. Again this is correlated with the strong arrival of a new phase, the SS-wave. Starting at the arrival of the first surface waves near $t = 1250s$, the linearity stays at a rather high level until approximately $t = 2400s$, where a strong vertical component of motion indicates the arrival of the Rayleigh wave. Once more, this behavior can easily be explained: The first surface wave to arrive is the Love wave. We expect the surface wave to be linearly polarized and hence show a high degree of linearity. The Rayleigh wave, on the other hand is elliptically polarized, which explains the sudden decrease in linearity.

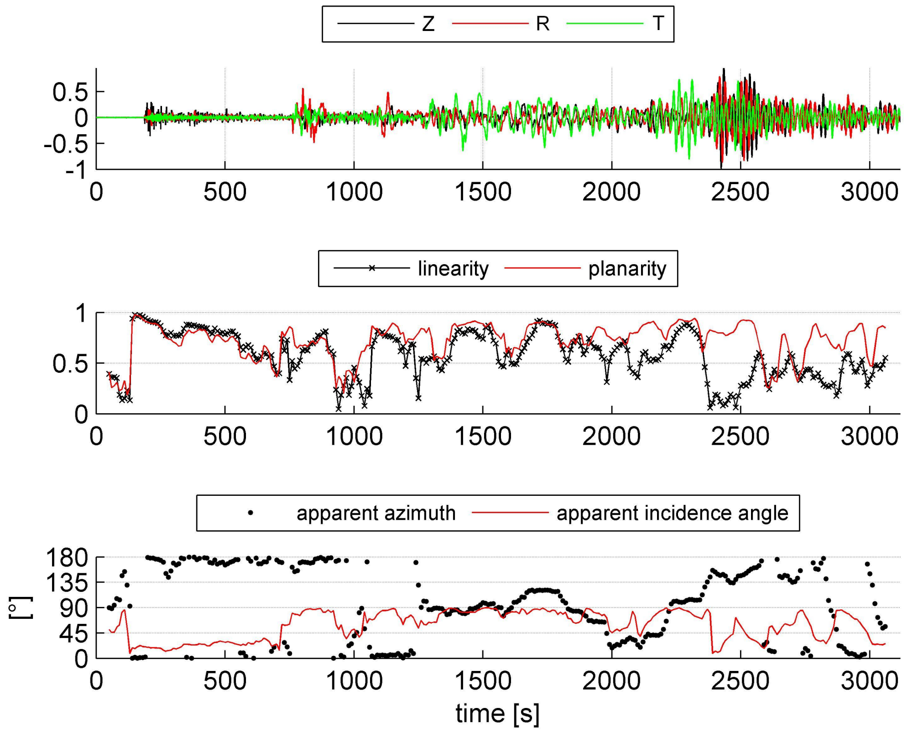

Figure 4.1.: Covariance matrix method; Polarization analysis of a global earthquake.

To understand the behavior of the planarity, it is necessary to recall that the definition was chosen such that the planarity is high whenever the linearity is high, but also attains a high value if the motion is confined in a plane. This explains the trend of the planarity very well. It follows the linearity up to $t \approx 2400$, where we expect the Rayleigh-wave arrival and hence a strong elliptical polarization. At that point, the high level of planarity together with the low linearity indicate that the motion is indeed confined to a plane and not distributed in 3D space, nor restricted to a linear motion.

We will now take a closer look at the apparent incidence and azimuth. During the P-wave coda, the incidence angle is very low, indicating an incidence from below. Since the P-wave motion is along the ray path and we expect the ray to emerge from depth, this is in accordance with the theory. With the first arrival of the S-wave the incidence angle jumps to nearly 90° indicating horizontal motion. This makes clear how important it is not to confuse the apparent incidence angle with the incidence angle of the ray. These can only be correlated for P-waves! It is even a consequence of the low incidence angle of the ray path that the apparent incidence of the S-wave is nearly 90°, as the S-wave should to be orthogonal to the direction of propagation. The apparent azimuth of the P-wave and the S-wave is approximately 0 (or 180; Recall that the apparent azimuth is only defined up to an uncertainty of ±180°). This is again in accordance with the theory, since our coordinate system was rotated from pointing to North and East, to point to the event and in transverse direction. An angle of 0° hence means that the main direction of motion points to or from the source. That the azimuth does not change from the P- to the S-wave is by chance and indicates that there is a strong SV component in the wave. However, that the azimuth is lower at the arrival of the SS-phase ($t \approx 1120s$) can again be explained. At the free surface, the SH-wave reflection coefficient is equal to 1, whereas the SV reflection coefficient is smaller than one. Thus, the SS-wave is more dominated by the SH-wave than the S-wave was, which leads to a rotation of the apparent azimuth away from its original direction along the ray path.

From $t \approx 1250s$ onwards, the azimuth is approximately 90° in good accordance with our assumption that the arriving wave is the Love wave. With the presumed arrival of the Rayleigh wave, the linearity takes on rather low values, the planarity rather high ones. This is a good indication for a Rayleigh wave arrival, since elliptical motion can be described by two vectors corresponding the semi-major and the semi-minor axis. These vectors correspond to the eigenvectors of the largest and the second largest eigenvalue when performing a covariance matrix analysis. We expect the Rayleigh wave to be retrograde, and both vectors should be confined to the plane with transverse component=0, leading to a theoretical azimuth of 0° (or 180°) for both the semi-major axis and the semi-minor axis. Note that the azimuth computed in the covariance matrix method always corresponds to the azimuth of the largest eigenvector corresponding to the semi-major axis. While we do not find exactly 0° or 180° for the azimuth as expected from theory, we do obtain values near to 180°.

It is instructive to investigate the differences between the covariance matrix method and the other closely related methods, the debiased covariance method and the complex covariance matrix method. Figure 4.2 shows a polarization analysis of the same data already used to produce Fig. 4.1, this time, though, using the debiased covariance method. Comparing Fig. 4.2 and Fig. 4.1, no significant deviation can be observed, even in direct comparison. This is not astonishing, since the mean was removed from the traces prior to the analysis and the time window is very large with $\Delta t = 100$s. Hence the mean of the windowed traces will be very small. Since both, the covariance matrix method and the debiased covariance method, work with the real seismic data and not with the analytic signal, we can anyway only expect to get correct values for the azimuth if we average over at least one wave cycle. In this case the difference between the two methods should be negligible. This will be especially true for local earthquakes, where the polarization content lies at low frequencies, but filters up to about 0.7Hz are required due to the seismic noise.

The next step is to compare the two previous methods with the complex covariance method. The polarization attributes for the event at Nicobar islands is shown in Fig. 4.3. Starting with the similarities: The apparent azimuth and apparent incidence angles obtained from the complex covariance method are more or less identical to those obtained from the covariance

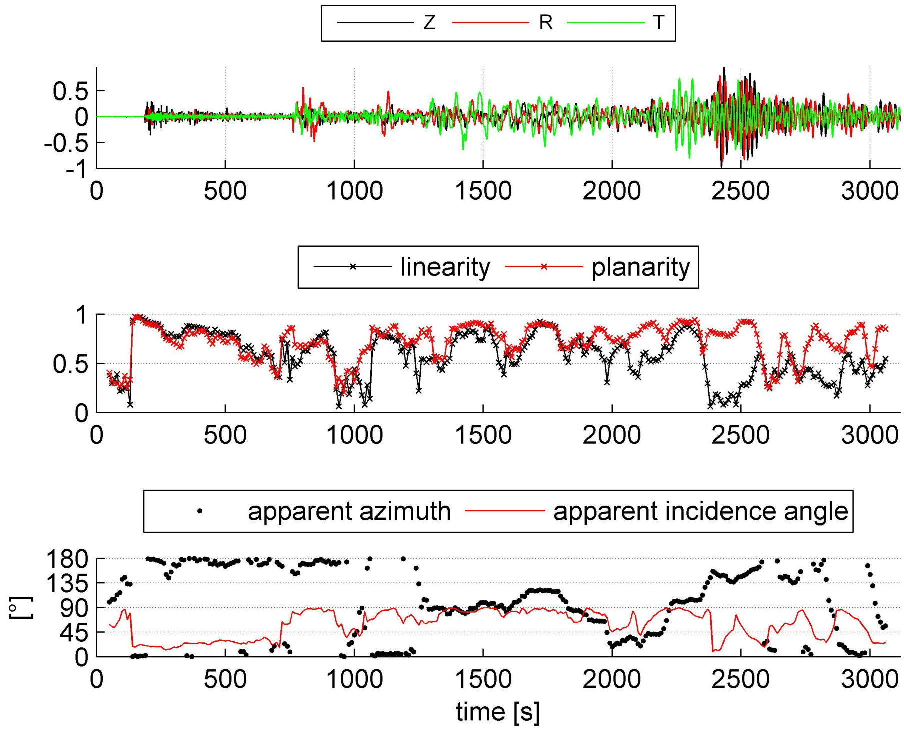

Figure 4.2.: Debiased covariance matrix method.

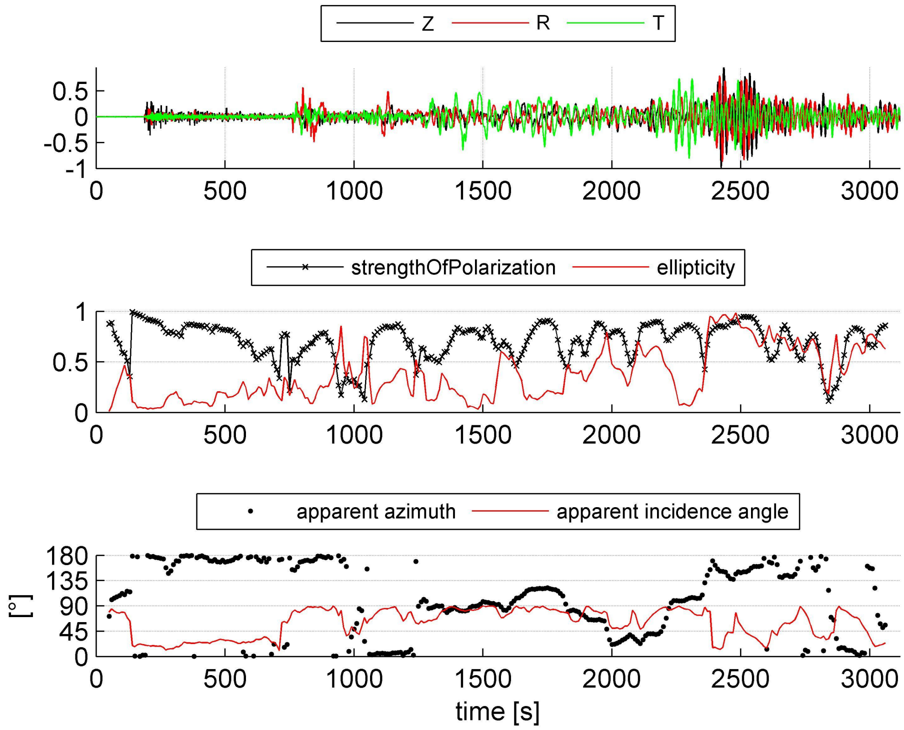

Figure 4.3.: Complex covariance method.

matrix method. Now let us examine the ellipticity and the parameter dubbed degree of polarization in Section 3.1.3 and in Fig. 4.3. The two parameters can easily be correlated with the linearity and planarity used in Section 3.1.1. Before explaining this, however, I want to stress once more that the term degree of polarization is somewhat misleading. The degree of polarization will be high if the linearity is high *or* if the linearity is low, but the planarity is high. Only if linearity and planarity are low, the degree of polarization will be low. The ellipticity will increase as soon as the planarity is higher than the linearity. There is a significant difference, though, between the planarity and the ellipticity: A high planarity indicates a high degree of polarization, the ellipticity, however, does not allow any inference on the degree of polarization. The ellipticity will be a meaningless attribute if the degree of polarization is low.

The complex covariance matrix method has advantages over the covariance matrix method when considering time resolution and necessary averaging times. This will be discussed in more detail at a later point (see Section 4.3).

The last coherency matrix method to discuss is the spectral matrix method (see Section 3.1.4). Other than the methods discussed so far, which all bear, up to a certain extent, similar information, the spectral matrix method allows for new information to be obtained. As an example see Figure 4.4, showing the onset of the earthquake already analyzed in Figures 4.1 to 4.3. As analysis parameters Δt was chosen to be 250s, the frequency window was chosen to be 6 samples, which corresponds to 6/250=0.024Hz. (The frequency window is only a function of the number of samples and the time window and is independent of the sampling frequency.)

The analysis window was chosen such that the first time window only contains data before the onset of the earthquake and the second time window includes most of the P-wave coda. This was done as to allow a good differentiation between noise and signal. The noise amplitude is high between about 0.1Hz

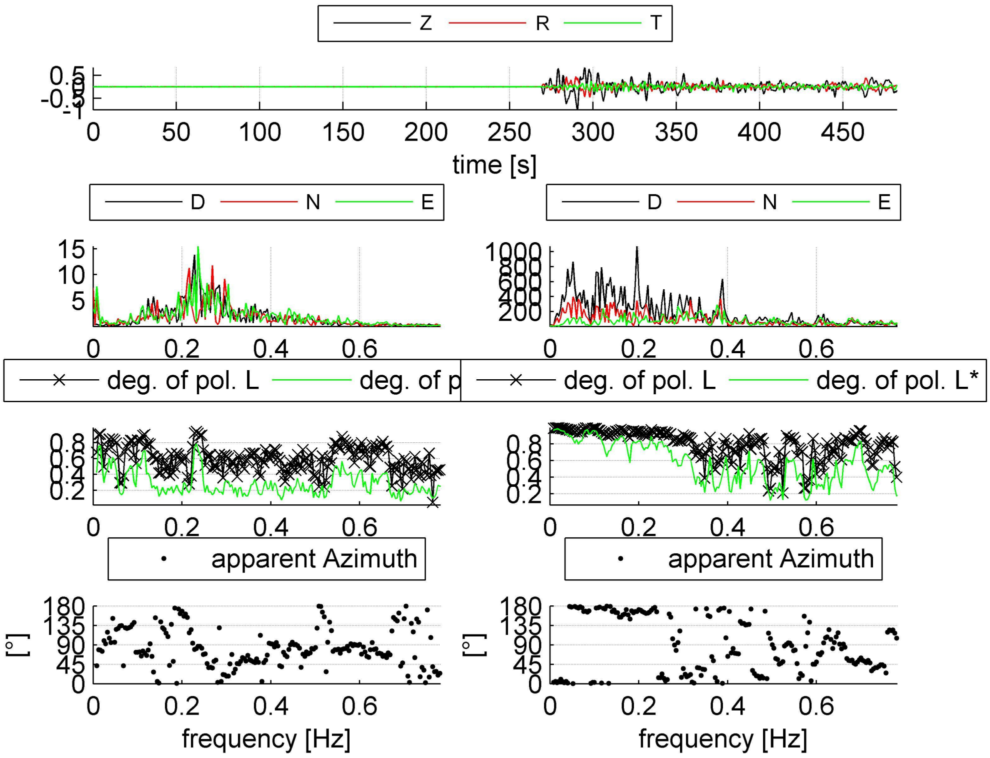

Figure 4.4.: Spectral matrix method.

and 0.3Hz. In this frequency range the degree of polarization is intermediate and the apparent azimuth fluctuates strongly. The signal is mainly present between 0Hz and 0.4Hz. However, the degree of polarization is only very high up to 0.25Hz, an interval in which the apparent azimuth lies stably around 0°. As discussed above, 0° is the apparent azimuth the theory predicts for the P-wave and is also the value obtained from the covariance matrix method and the complex covariance method, although those methods include all frequencies. That 0° could be recovered by the two last named methods, is due to the fact that the polarized part outweighs the less polarized part at higher frequencies. Nonetheless, the presence of unpolarized parts in the signal decreases the linearity and the degree of polarization in the covariance matrix method and the complex covariance matrix method. Applying a filter prior to the analysis would hence be favorable. The complex covariance matrix method may give information on how to choose this filter. Figure 4.5 clearly shows the positive effects of such a filter. The degree of polarization goes up and the azimuth stays more stable. This example makes clear how the spectral matrix method can aid other methods. In spite of this, the method is not highly practicable as stand alone method, especially if the time sequence is long and contains different signal types making a certain time resolution necessary. In such cases, the STFT-method (see Section 3.4) may be preferable. It is a fast computing method and is somewhat related to the spectral matrix method as it also makes use of the signal's Fourier transform. In the implementation of this method, the degree of polarization is not explicitly calculated. However, as discussed in connection with the S-transform method (see Section 3.3), the user can compensate this by looking for arising patterns. Figure 4.6 shows the result of such an analysis. Looking at the plot titled "semi-major/semi-minor", i.e. the ellipticity plot, we can clearly see the P-wave arrival (blue colors signifying very low ellipticity) and the S- and SS-wave arrivals (in red), separated by yellow-greenish regions. In the amplitude plot (second line on the left) we can then clearly see a

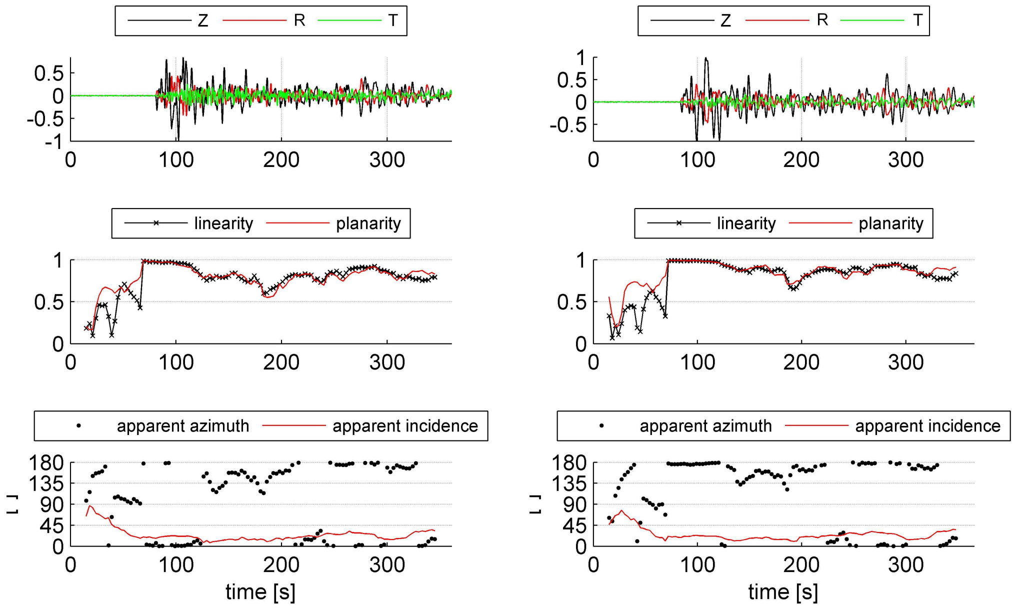

(a) No filter applied.

(b) Filter: 0.03Hz-0.25Hz, Butterworth filter, 2 poles

Figure 4.5.: Covariance matrix method: Comparison of results with and without a filter deduced from the spectral matrix method

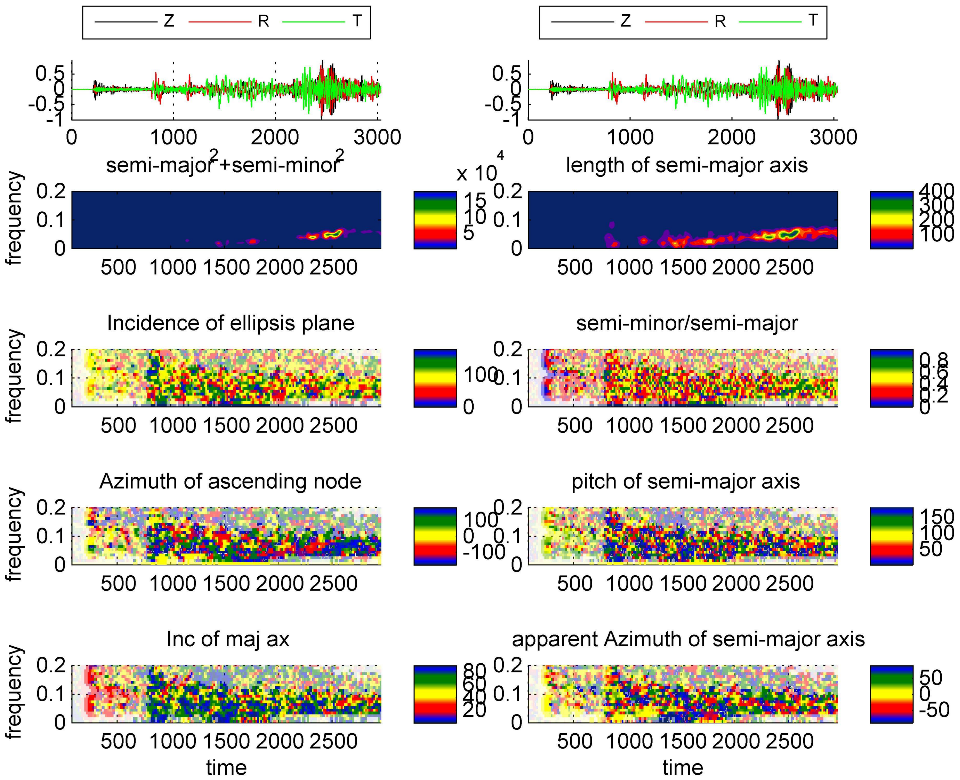

Figure 4.6.: Short time Fourier transform method.

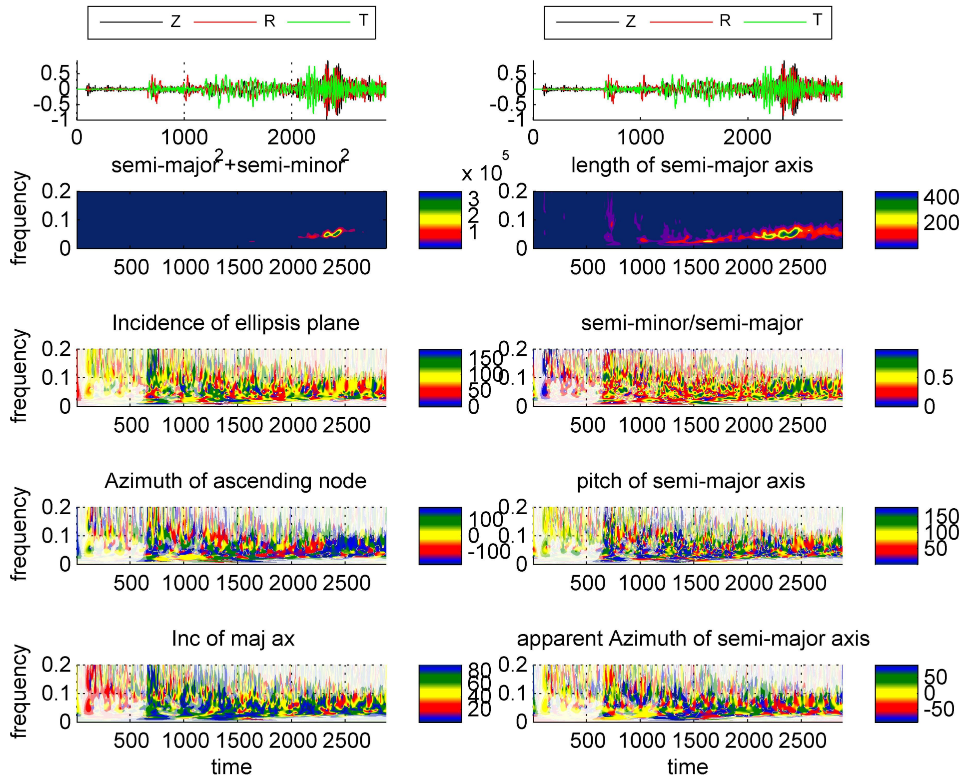

Figure 4.7.: S-transform method.

dispersive signal. The signal is at first linearly polarized, with comparably small ellipticity values (blue, red and yellow). At $t = 2500$s the ellipticity becomes very high (green patch). This high ellipticity corresponds to a blue patch in the "azimuth of ascending mode" plot and a yellow patch in the "incidence of ellipsis plane" plot indicating retrograde motion, as expected for a Rayleigh wave. Only the "pitch of semi-major axis" does not totally conform to the theory, which predicts a stable value at 90°.

Similar information can be obtained from the S-transform method (see Fig. 4.7 for an example of an S-transform result). The similarity is due to the small frequency bandwidth of the signal. However, the S-transform method still has the advantage of optimizing the time-frequency resolution (the changing time resolution is shows clearly in Fig. 4.7; the patterns become much more elongate in vertical direction with increasing frequency indicating a better time and a worse frequency resolution.) In spite of this advantage, the method has one profound disadvantage: it is computationally much more complex and the trace has to be resampled prior to the analysis (it this case to 0.4 samples per second). Fourier artifacts show up at the beginning of each plot: A blotch bounded by something looking like a $1/t$-function. This is due to the fact that the time window slowly slides into the time-sequence. Since the time window is shorter at higher frequencies, the artifacts diminish faster at high frequencies.

4.2. Local Earthquake Data

4.2.1. Dataset

As next step, I investigated local earthquakes showing frequency contents approximately between 1Hz and 15Hz. Although the polarization of higher frequency waves is more easily influenced by the subsurface structure due to the smaller wave lengths, we still expect to find meaningful parameters, such as the polarization of the P-wave, which should approximately point back to the location of the earthquake [22].

In the analysis of the local earthquake data, I focused on the covariance method and the complex covariance method, only using the other methods for comparison (and sometimes to gain additional information). Again, the analysis worked well, showing all expected features as discussed below for the example of an event with a body wave magnitude 4.3 of located near Mürzzuschlag, Austria. All data from broad-band stations maintained by the Zentralanstalt für Meteorologie und Geophysik, Austria was considered, specific examples are given for the MOA station.

4.2.2. Discussion

Figures 4.8 and 4.9 show the result of the analysis using the complex covariance matrix (see Sec. 4.3) and the spectral matrix method (see Sec. 4.4). Prior to the analysis the mean was subtracted from the data, and the traces were rotated to radial and transverse direction. In the case of the complex covariance matrix method, the data was filtered to 0.5Hz-2Hz; the time window used in the analysis was 2s. The most striking feature in local earthquake

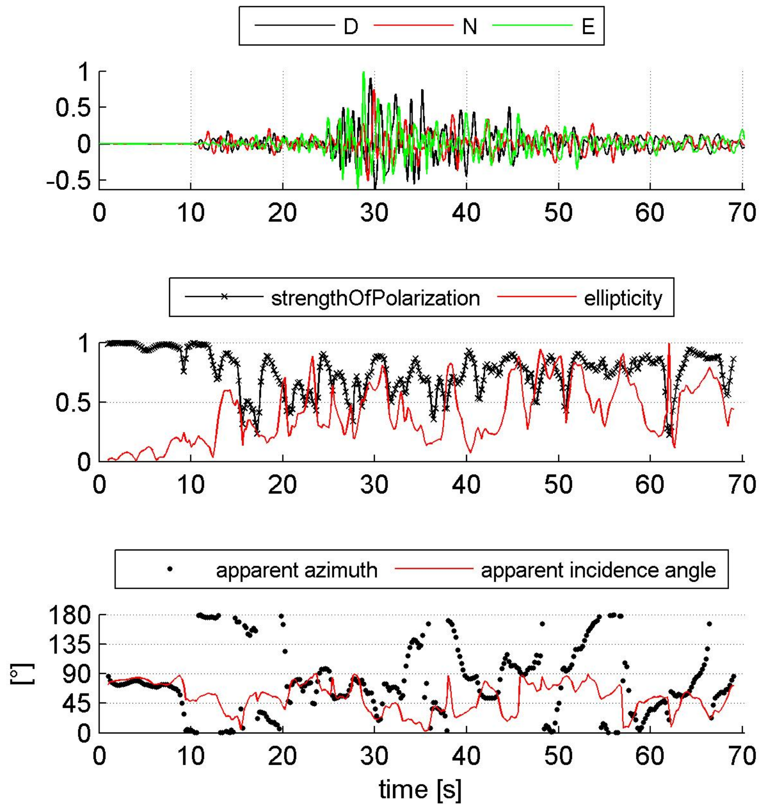

Figure 4.8.: Local earthquake; complex covariance matrix method.

data is usually a very high degree of polarization at the P-wave onset. As an example, see Fig. 4.8, where the P-wave onset at $t \approx 10$s is marked by a degree of polarization around 1 and a very small ellipticity. In the region

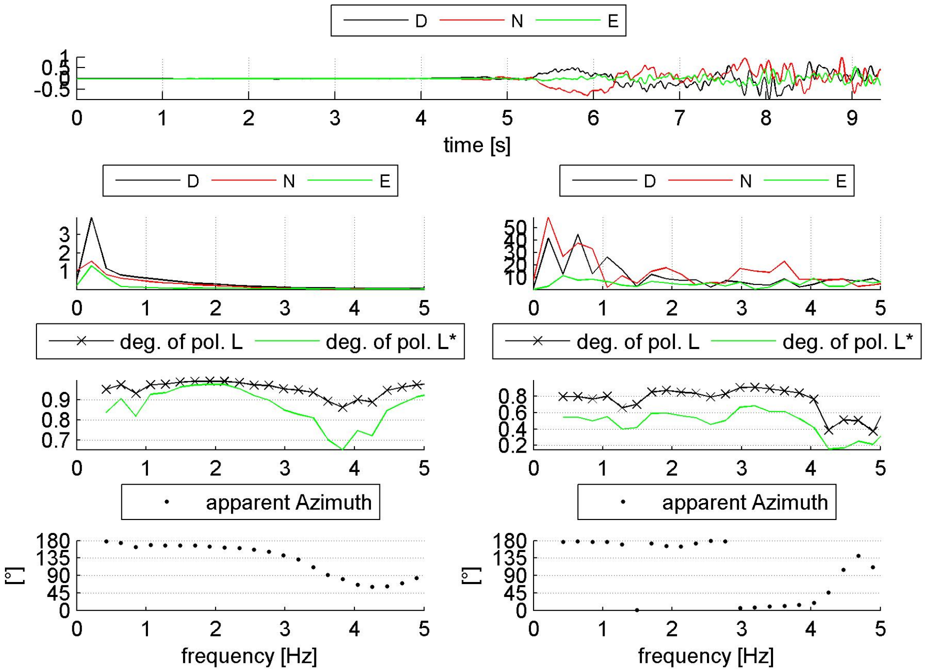

Figure 4.9.: Local earthquake (onset of P-wave); spectral matrix method.

where the degree of polarization is high, the azimuth is stable and points approximately into the direction of the source location. The high degree of polarization before the P-wave onset is probably due to noise and can indeed be reduced by filtering the data from 1Hz to 3Hz instead of from 0.5Hz to 2Hz, but with the undesirable side effect of also slightly lowering the degree of polarization of the P-wave onset. Although the polarization of the P-wave is typically strong in local earthquake data, it should be noted here for future reference that this is not always the case. Small degrees of polarization were usually obtained if the P-wave amplitude is very small and the onset is smooth. In some other cases, the azimuth does not stay stable over a sufficiently long period as to allow an identification of a specific value to the onset; other results simply show a low degree of polarization, implying that several wave types arrive simultaneously.

4.3. Influence of the time window on the results

As noted before (see Sec. 2.1.2), the time window used in the covariance matrix method, the debiased covariance matrix method and the complex covariance matrix method has a great influence on the result. Especially for the covariance matrix method and the debiased covariance matrix method, which are not based on the analytic signal, choosing a "correct" averaging time is crucial. Figures 4.10 and 4.11 make this clear. The former compares the results for the covariance method analysis the P-wave onset of an earthquake near L'Aquila, Italy, with a magnitude of 3.9 [21] recorded at the Conrad observatory, Austria, the latter the results for the complex covariance matrix method. I will first discuss Fig. 4.10. For very short averaging times, the linearity and the planarity are, not surprisingly, approximately equal to one. The azimuth approximately follows the instantaneous displacement for extremely short averaging times such as $\Delta t = 0.025$s, since the main frequency content of the data is around 2Hz, corresponding to a period of $T = 0.5s$. In spite of the high degree of polarization, the values of the azimuth are thus meaningless! At $\Delta t = 0.2$s a slight modulation of the azimuth and incidence with the main period can still be observed. These modulations level out as soon as the averaging time is greater than one full wave cycle. At $\Delta t = 0.5$s the azimuth is still very unstable, a longer averaging time might thus be desirable, although information is then lost.

The complex covariance method shown in Figure 4.11 does not have the same problems, of the azimuth following the instantaneous displacement since this method makes use of the analytic signal. The wild oscillations observed for $\Delta t = 0.025$s in Figure 4.10 between 12s and 20s disappear, the value of the azimuth and incidence are always meaningful, but may be difficult to interpret. For a straight forward interpretation I always tried to find an averaging time where the degree of polarization shows strong dependencies

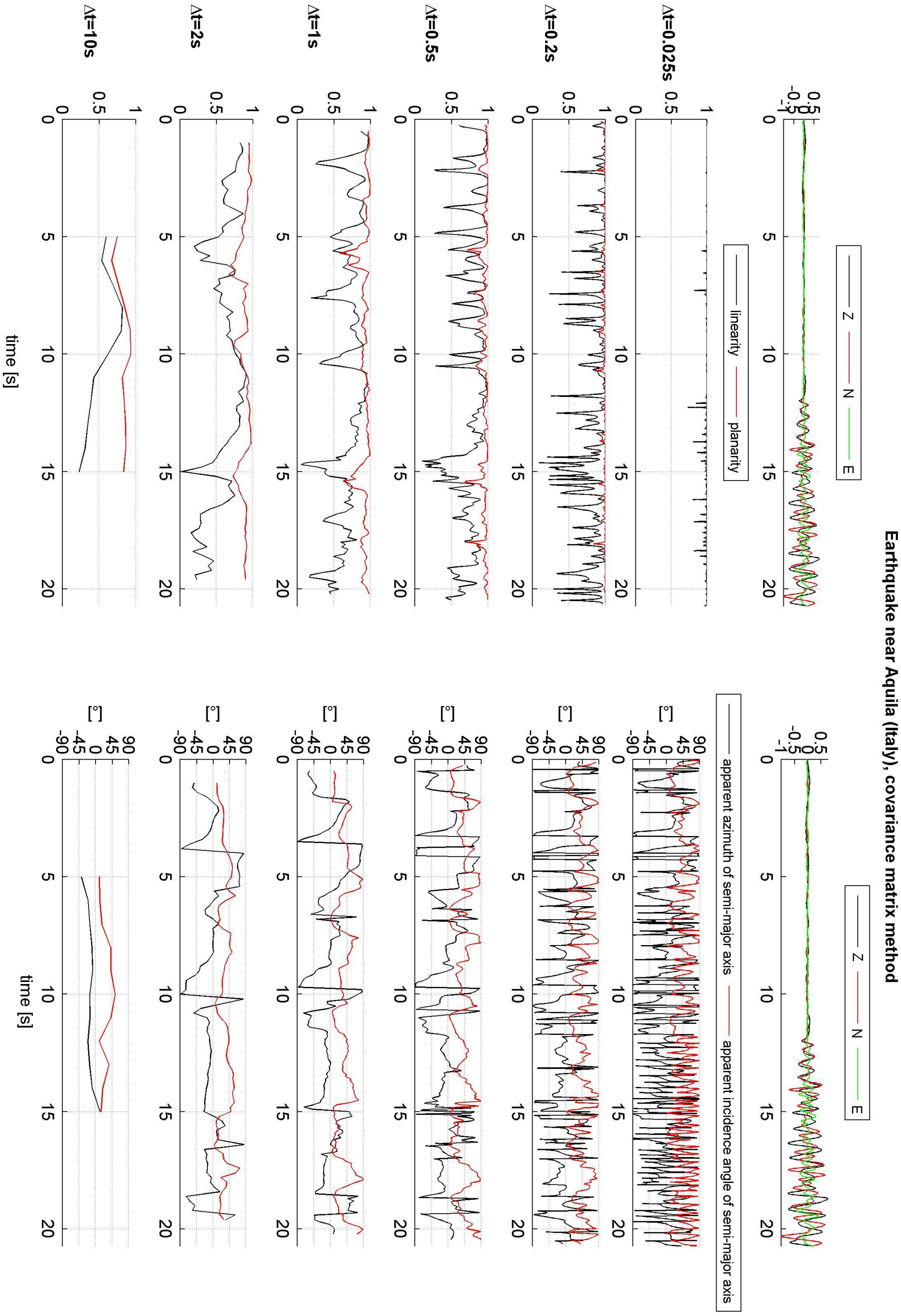

Figure 4.10.: Comparison of different averaging times used in the covariance matrix method to analyze local earthquake data.

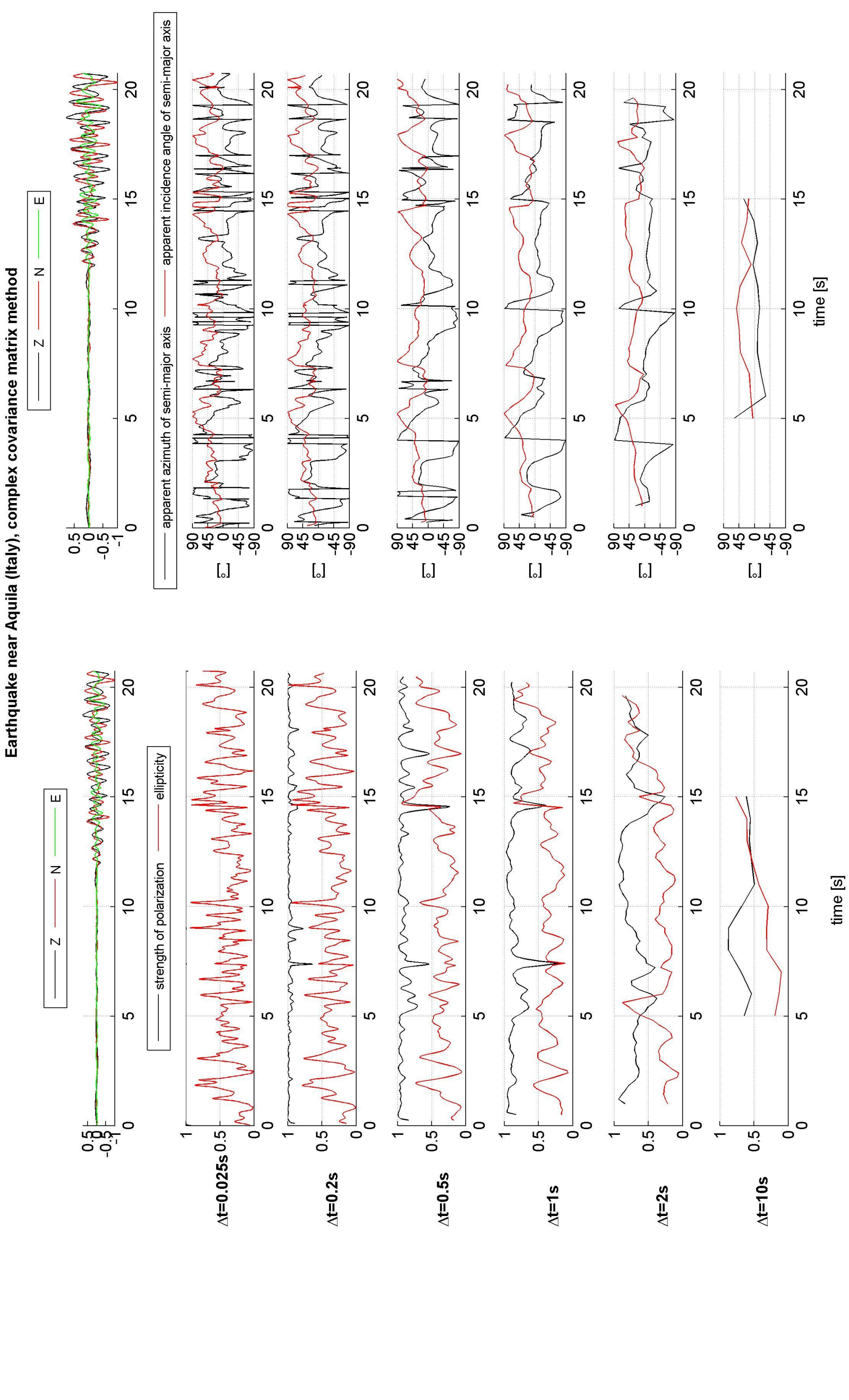

Figure 4.11.: Comparison of different averaging times used in the complex covariance matrix method to analyze local earthquake data.

on the data and the azimuth is slightly stabilized. This would be fulfilled at $\Delta t = 1$s in this case. Much longer averaging times (such as $\Delta t = 10$s) would not be desirable since the time resolution is then lost.

4.4. Advantages of polarization analysis over re-orientation

After having discussed the implemented methods and their information content, it is important to debate the advantage of the polarization analysis over the mere rotation of the data to the source.

Reorientation of the seismic data to the source is common practice: up-down, north-south and east-west components are rotated in the horizontal plane to up-down, radial and transverse components. This is advantageous in oder to be able to discern different wave types. Although much information can indeed be deduced from mere re-orientation, the polarization analysis does provide certain advantages.

Foremost and most obvious is the fact that the polarization analysis allows a quantization of otherwise rather subjective impressions. While the human eye is able to correlate "wiggles", the gathered impressions depend on the persons experience as well as his or her abilities. Every method of polarization analysis leading to a "degree of polarization" or a "degree of linearity" will quantize these impressions and hence provides an objective measure.

A second advantage is the possibility to analyze the polarization attributes, i.e. the apparent incidence angle, the apparent azimuth, and all parameters fully describing an ellipsis (these parameters were calculated in the STFT-method and the S-transform method only, but can, in principle, be obtained from the complex covariance matrix method and the spectral matrix method too). An obvious application of these parameters is to check if a potential

Rayleigh wave does indeed show retrograde motion (as was done in Section 4.1.2, when discussing the STFT-method). Another example would be to test if the P- and the S-wave are indeed orthogonal. This can easily be done using any of the covarinace matrix methods opperating in the time domain. By specifying a time window which is dominated by the P-wave onset, the semi-major axis (or main direction of motion) can be compared to the semi-major axis (or main direction of motion) of time-windows covering the rest of the trace. A simple test for orthogonality is to compute the inner product of the two resulting vectors, this is proportional to the cosine of the enclosed angle. Figure 4.12 shows an example using the covariance matrix method. Clearly, the S-wave is orthogonal to the P-wave.

Less obvious is the fact that even the azimuth and incidence angles calculated in the polarization analysis themselves provide new information compared to reorientation only. Naively, one would think that the amplitude of the transverse to the radial component should be related to the apparent azimuth. However, this is not true. A good example is the P-wave onset of the earthquake analyzed in the last section: Figure 4.13 shows the reoriented traces. Performing a polarization analysis of these traces, we find an apparent azimuth of appoximately $0°$. The traces, however, give a different impression. Even considering the scales (the maxima and minima of the shown traces are given in counts on the left of the graph), the radial component only appears to have about double the amplitude of the transverse component. This naive approach would give an azimuth $\theta = \arctan \frac{1}{2} =\approx 26°$, very different from the true azimuth of $\approx 0°$. This difference comes from the fact that the radial component is strongly correlated with the (very strong) Z component as can be seen in Fig. 4.13. The Z and the radial component can thus approximately be described by one vector with varying amplitude. The transverse component has to be described by a separate vector, since it shows a different evolution in time. But since the Z and radial component taken together have much greater amplitude than the transverse component alone, the vector de-

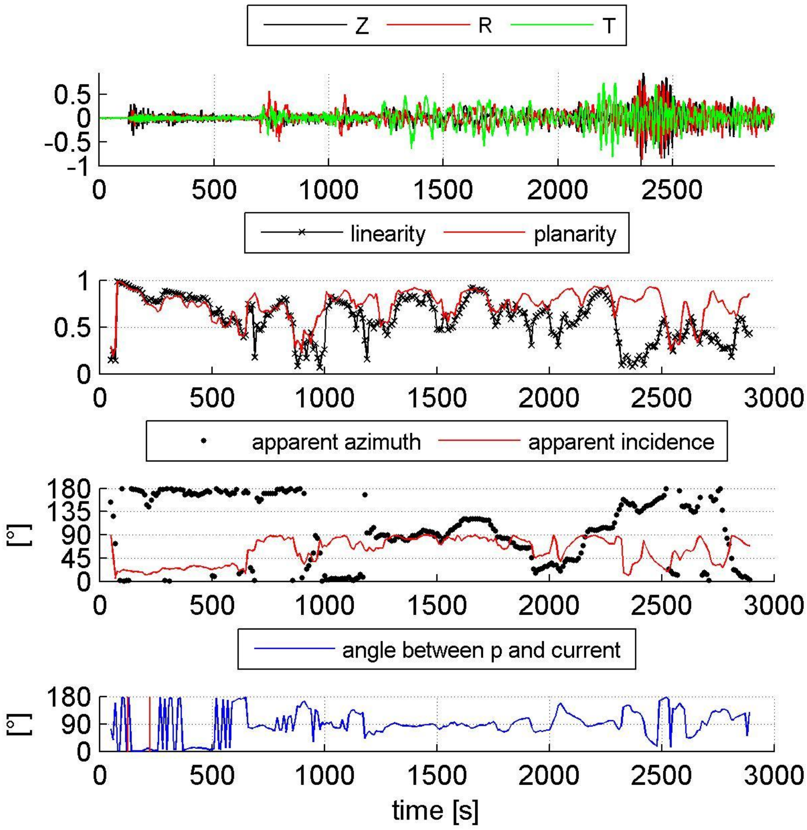

Figure 4.12.: Covariance method, with additional “is orthogonal” analysis.

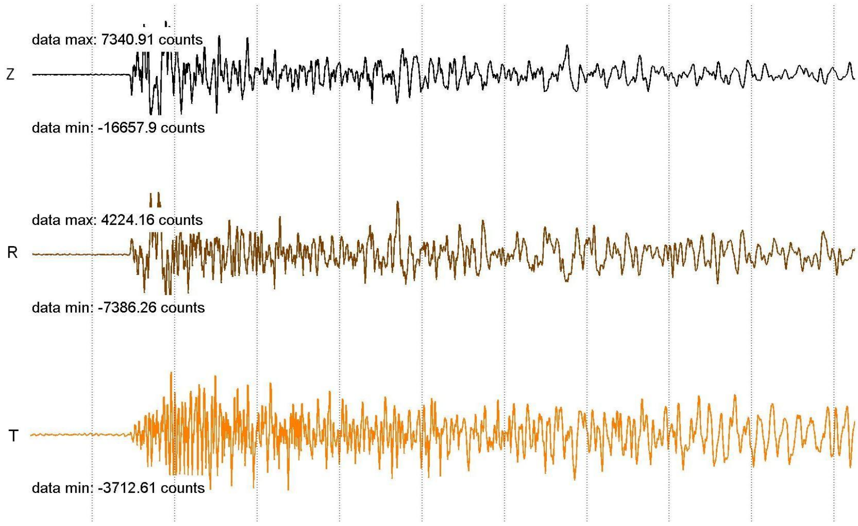

Figure 4.13.: Reoriented traces of P-wave onset

scribing the radial and Z component will be the one corresponding to the largest eigenvalue (in the case of the covariance matrix methods) and will hence define the apparent azimuth. This vector, however, obviously has a negligible transverse component, leading to an apparent azimuth of approximately 0°. This example shows well how an analysis including a polarization analysis can outperform an analysis simply using reorientated traces.

5. Application to Short Period Data

I have shown in the last chapter that it is possible to extract information on the seismic wave polarization from three component data by using the methods implemented for SEISMON in the course of this work. So far, however, the methods were only applied to global and regional earthquake data. In this chapter the applicability of the methods to short period data will be investigated.

5.1. Datasets

As sample data I used data recorded at a mass-movement in Gradenbach. Gradenbach is located in the Schober mountain range, south of the central Eastern Alps near Döllach[23]. In 1965 and 1966 the mass-movement triggered catastrophic debris flows and has been under geophysical investigation ever since [23, 24].

No broad-band seismometers are available at Gradenbach. The seismic data is recorded by 1 and 4.5Hz geophones, which are situated in a highly complicated topography and are not installed on solid rock, but are buried in the ground.

5.1.1. Local earthquake data

Data from local earthquakes with magnitudes between 1 and 4 recorded with the geophones at Gradenbach were used in preliminary investigations described in Section 5.3.

5.1.2. Short period data originating from the landslide

Data recorded at Gradenbach has been analyzed, reduced as far as possible to events related to mass movements on th slope, ordered according to the type of events, and cataloged by Stefan Mertl [25]. Consequently, I had access to data presumably originating from the hillside, which I used for my investigation.

5.2. Preliminary Work

Since, in the prvious investigations, the polarization was often found to be stronger in the lower frequency content, a first necessary measure was to extend the geophones' bandwidth to the frequencies expected in local earthquakes, i.e. approximately 1Hz. This could be accomplished filtering with the inverse of the geophones instrument response together with a high-pass filter with a cutoff frequency of 0.7Hz. The latter is necessary to stabilize the inverse filter and to prevent the usage of data distorted by an instrument response that does not follow the exact response predicted for a geophone with a certain damping parameter anymore.

5.3. Investigating Subsurface and Topography influences

The first question arising was if the data from Gradenbach shows polarization at all. The stations in Gradenbach are situated directly at the (inclined) surface and are installed on an extremely weak subsurface due to the loosening of the ground in the region of the land-slide. The first may have important consequences since the waves will reflect from the surface, leading to a superposition of waves which may easily disturb the polarization. The second point has consequences for the ray path. In weak ground, the ray may scatter, bend and superimpose, which could lead to depolarization. Furthermore, the complicated subsurface structure may enhance wave conversion.

In order to investigate if polarization attributes can actually be observed in the data recorded at Gradenbach, I made use of a fact stated in the last chapter: the typically high linearity or degree of polarization of the P-wave onset with an apparent azimuth pointing back to the source location. The polarization was measured using the covariance matrix method with time-windows between 1s and 2s and a 95% window-overlap. A polarization value was rejected, if the linearity was not higher than 0.65 and the planarity was not lower than 1.4 times the linearity for at least 4 sliding windows in the near vicinity of the picked P-wave onset. Furthermore, the polarization attributes were rejected if the azimuth changed too rapidly. The data was filtered prior to the analysis, typically with filters from 0.7Hz to 2Hz or from 1Hz to 3Hz, depending on the frequency content of the data.

Applying these rules to data recorded at Gradenbach, the polarization could very often not be determined. Therefore, I chose always to consider a cluster of several earthquakes located close to each other, such that the individual backazimuths at each station form a cone with a narrow opening angle. We hence expect the P-wave's apparent azimuth of each earthquake within one cluster to point in approximately the same direction. Three such clusters were considered, the choice of clusters being slightly limited by the fact that for such an analysis, several large enough earthquakes have to have occurred in a small region within a rather short time period determined by the time the geophones at Gradenbach were installed. The three clusters considered lie near Innsbruck, Austria, in a north-westerly direction from Gradenbach; in the Friaul, Italy, to the south of Gradenbach, and in Poland, to the north-east of Gradenbach. The results of these investigations are shown in Figures 5.1 to 5.3. On the basis of these figures, we can make the following important observations:

- In spite of the inhomogeneous subsurface, the surface-near installation of the geophones, and their high cutoff frequency, it is possible to obtain meaningful results for a polarization analysis at Gradenbach in the sense that the P-wave onset of events located close to each other typically show the same main direction of motion. This can easily be seen by the fact that the colored lines in Figures 5.1 to 5.3, representing the apparent azimuth, typically point to a similar direction.

- However, the polarization is weaker at Gradenbach compared to neighboring stations. This statement is grounded on the fact that the polarization at the Gradenbach stations could be measured less frequently, since the criteria set for the determination were less frequently met. This fact also shows up in Figures 5.1 to 5.3: although there are six stations situated close to each other at Gradenbach, there are typically not six times as many colored lines (depicting the main direction of motion) at the six Gradenbach-stations than at the other (single) stations.

- The measured direction of motion is biased, showing a systematic offset from the true azimuth. This is mainly true for the Friaul cluster, where the events are located south-south-westerly to south-easterly of

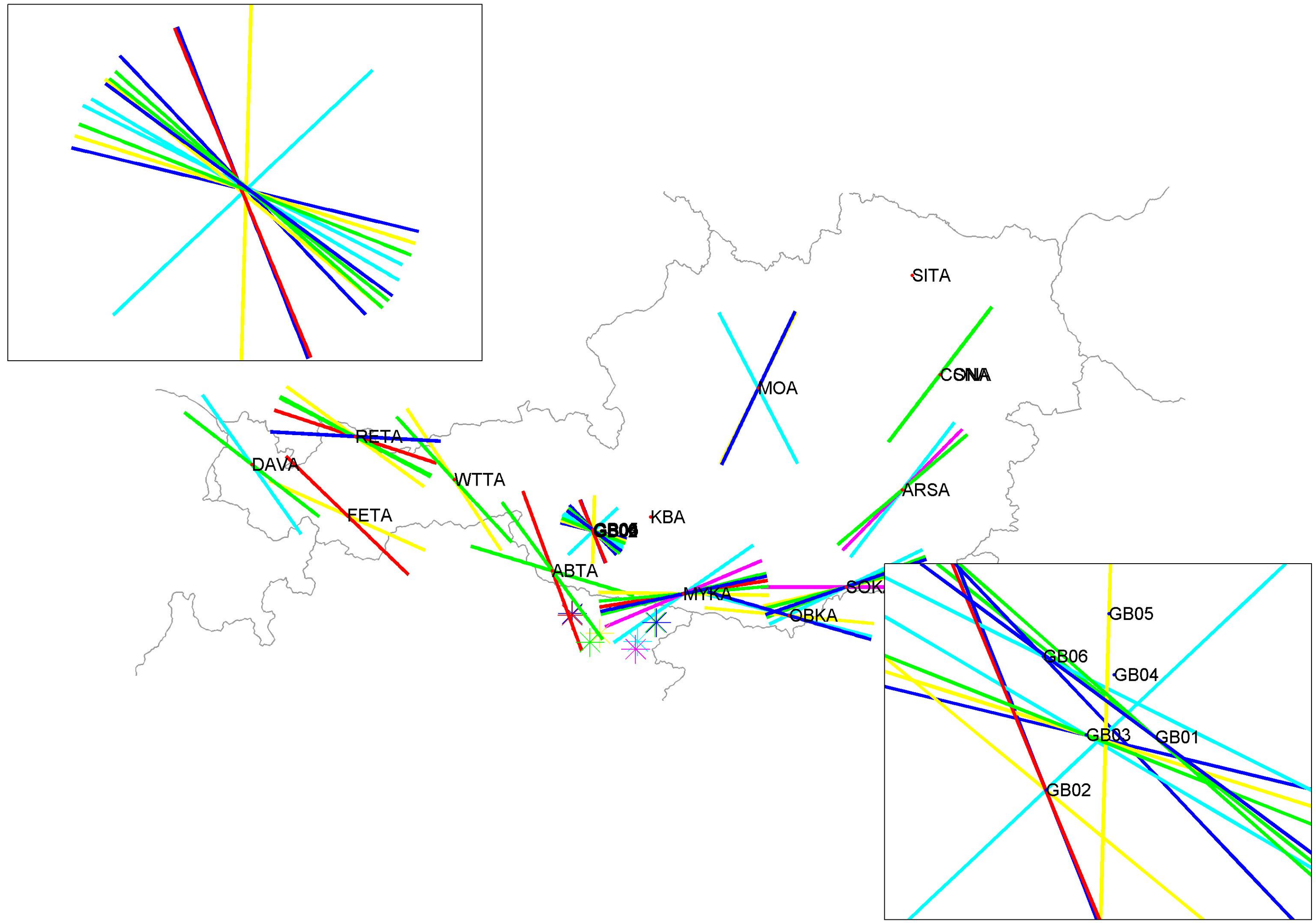

Figure 5.1.: P-wave polarization for several earthquakes located in the Friaul region, recorded at Gradenbach and several other Austrian stations. The insets are zoomed-in views of the stations in Gradenbach (upper left: 20km×20km; lower right: 2.5×2.5km). Each color depicts the results for one earthquake whose location is represented by a star in the same color.

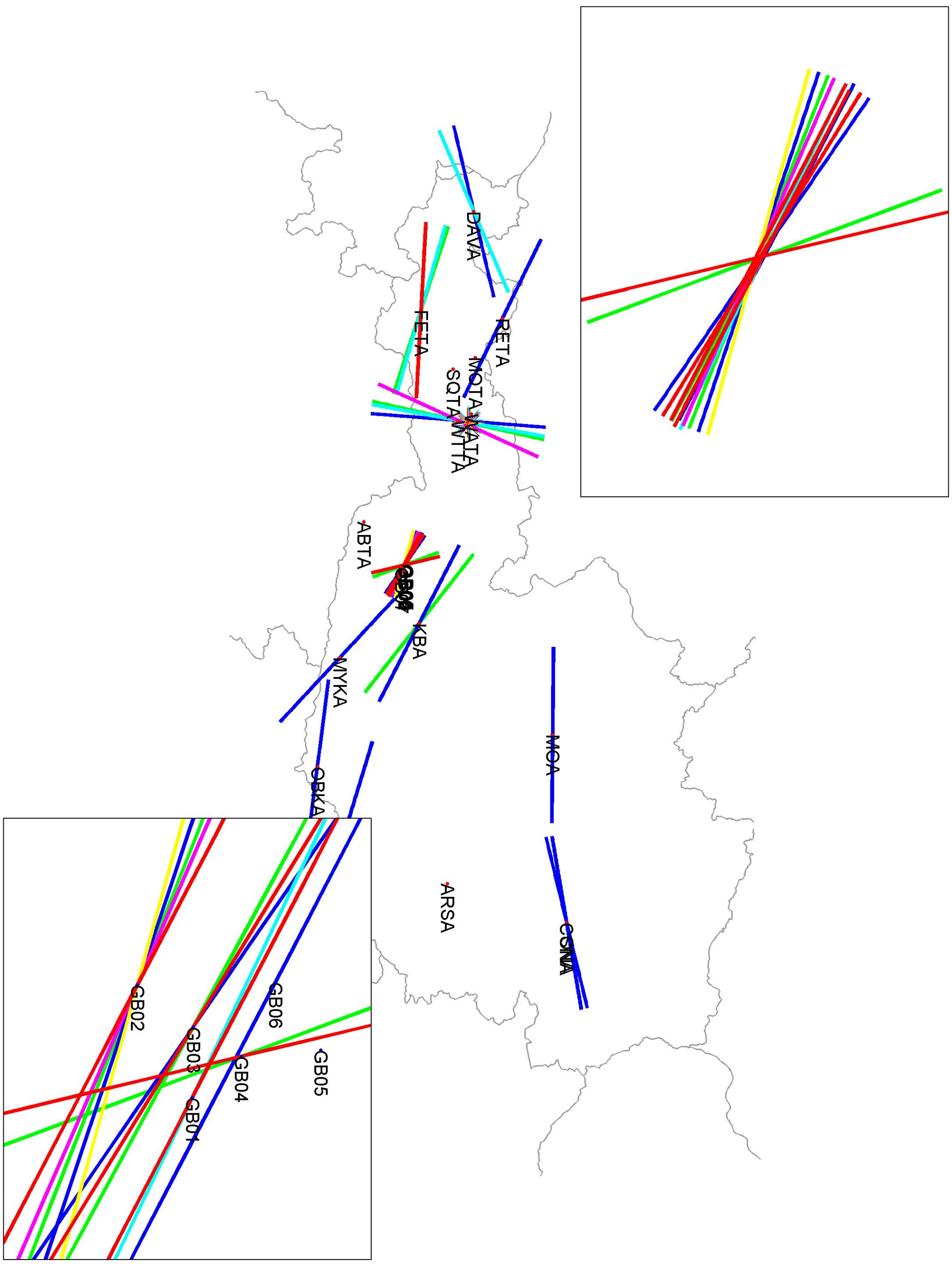

Figure 5.2.: P-wave polarization for several earthquakes located near Innsbruck, recorded at Gradenbach and several other Austrian stations. The insets are zoomed-in views of the stations in Gradenbach (upper left: 20km×20km; lower right: 2.5×2.5km). Each color depicts the results for one earthquake whose location is represented by a star in the same color.

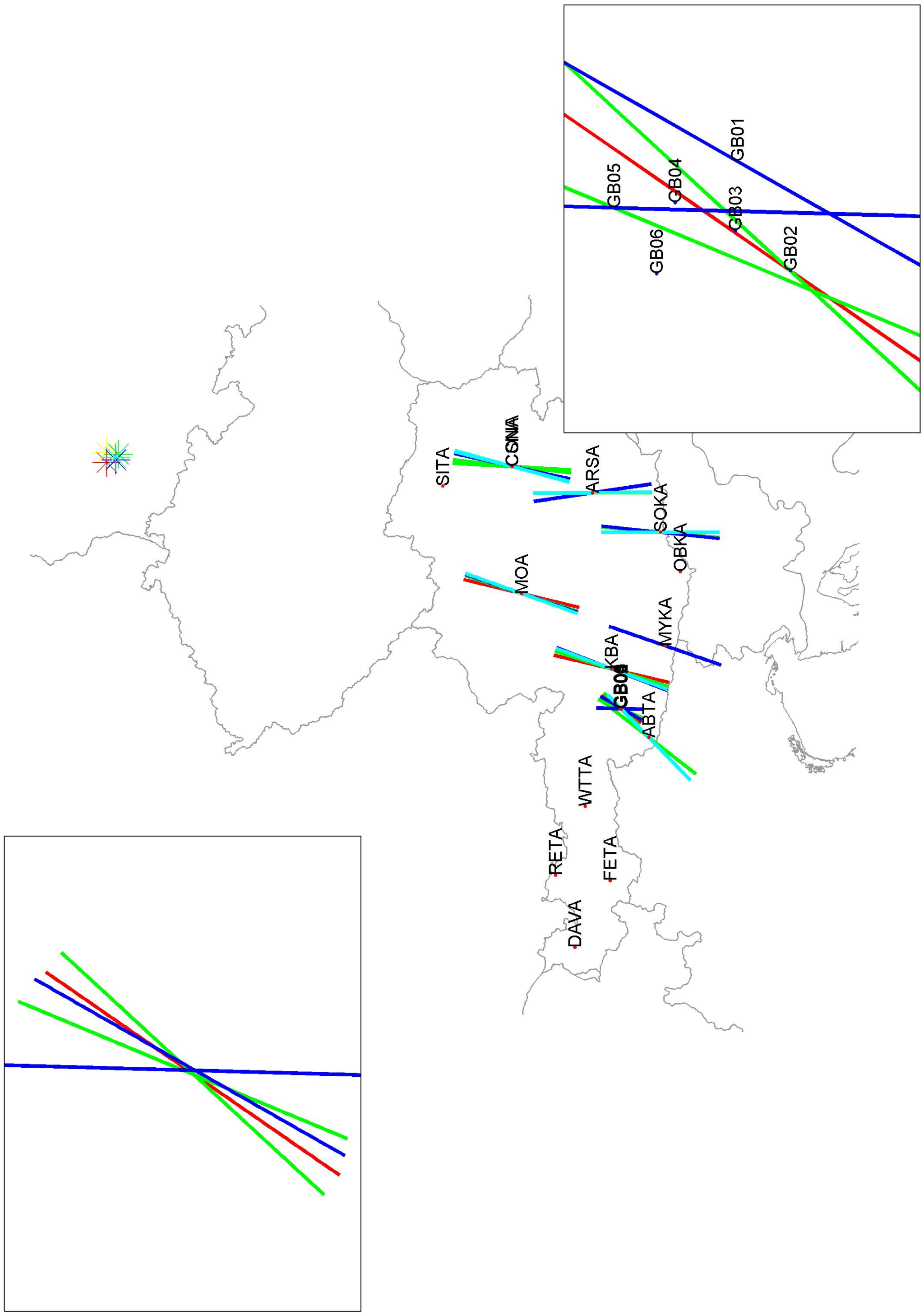

Figure 5.3.: P-wave polarization for several earthquakes located in Poland, recorded at Gradenbach and several other Austrian stations. The insets are zoomed-in views of the stations in Gradenbach (upper left: 20km×20km; lower right: 2.5×2.5km). Each color depicts the results for one earthquake whose location is represented by a star in the same color.

the stations but the measured direction of motion typically points to directions from south-east to east-south-east (see Fig. 5.1). This behavior can, however, also be observed for other stations (e.g. MYKA or ARSA in Fig. 5.1) (These stations were filtered by a high-pass filter comparable to that applied to the Gradenbach stations, so as not to have spurious effects of lower frequencies which could also be measured by these broad-band stations). A possible reason is ray bending on a large scale - this would have to be reflected in biases at other stations in Austria too. As can be seen from Figure 5.4, the Austrian stations show a much smaller bias. (That the median is closer to zero does not necessarily indicate a smaller bias, since the bias could be random at different stations throughout Austria. However, the fact that even the most extreme data points of the Austrian stations are closer to zero than the median of the stations in Gradenbach necessitates a stronger bias for the Gradenbach stations.) This makes it unlikely that large scale ray bending is responsible for the bias.

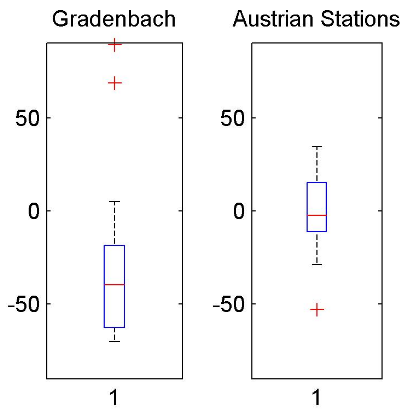

(a) Friaul cluster

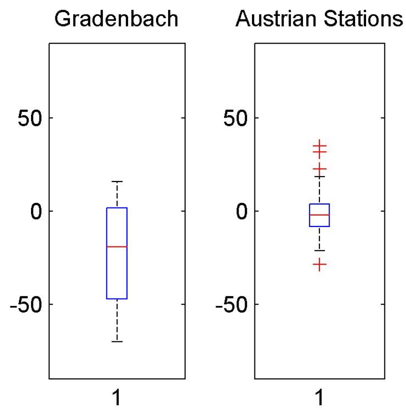

(b) Poland cluster

Figure 5.4.: Boxplots for the Friaul and the Poland cluster; red lines: median, blue box: 25% and 75% percentile, black lines: most extreme data points not considering outliers (red crosses).

Alternatively, rays arriving at Gradenbach from specific directions might be reflected, refracted or converted consistently for all stations. Consistency for all stations could result from the fact that all stations are situated on a similar slope and the main velocity contrast, separating the loosened material from the hillside is approximately parallel to the slope [24].

- Additionally to the systematic offset, there are several strong deviations between specific measurements and the mean direction of motion. This can be due to the local subsurface and surface structure, leading due to local ray bending (an effect that should be less pronounced at low frequencies), due to local scattering or to local wave conversions.

5.4. Investigation of short period data

Having shown that the polarization content of the data recorded at Gradenbach is not completely lost due to subsurface and topography influences, the use of polarization analysis for short period data from Gradenbach could be investigated. The question was in what extent the use of three component data can aid seismic monitoring and investigated seismic data attributed to sliding events at the hillside.

Three types of events triggered my special interest: Type AA and Type B events as well as two rockfall events (one known and one suspected). The AA events and the rockfall events were of interest since they show a strong onset, which is favorable when trying to measure the P-wave polarization. If the onset corresponds to a P wave, its direction of motion is expected to lie close to the true azimuth. This would enable constraining the event's origin by the crossings of the polarization directions.

Unlike the regional earthquakes, where the main frequency content lies between 1Hz and 5Hz, the frequency content of the AA events' onset typically lies much higher. This brought up a new problem: Probably due to resonances in the solar energy system supplying the system with electricity, there are three strong parasitic frequencies in all data from Gradenbach taken at daytime. These parasitic frequencies have a great influence on the measured polarization, since they are very mono-frequent and thus show a high degree of polarization (see Section 3). The disturbance typically lies around 28Hz and multiples thereof. These frequencies have to be eliminated prior to any analysis containing frequencies including such spurious amplitudes. This was achieved by applying narrow-band zero phase filters with two poles at each parasitic frequency additionally to a 1Hz high pass filter applied to diminish low frequency seismic noise. Another problem arose due to the shortness of the events. In order to allow an investigation with shorter time windows ($\Delta t = 0.3$), the complex covariance method was used throughout the following investigations.

Figures 5.5(a) and 5.5(b) show the measured main direction of motion of two AA event's onsets. Figure 5.5(c) shows randomly generated lines through each station. Figure 5.5(d) shows the result of localization of the first three events (Figures 5.5(a) to 5.5(b))performed by Stefan Mertl by means of relative P-wave travel times [25]. At a first glance it may seem that the line crossings in Figures 5.5(a) and 5.5(b) represent the source locations shown in Figure 5.5(d) quite well. However, we would also have to take those crossings into account which lie so far outside the Gradenbach region that they are not shown in the plot any more. In both cases shown, the crossings are even wider spread than those in Figure 5.5(c) showing randomly generated lines. Obviously the onset's main direction of motion shows such high deviations from the true azimuth, that they cannot be used for a localization of events. The reason for this "inconsistency" can be any of the reasons discussed in connection with the cluster analysis, or that the onset is not characterized by mainly P-wave coda. In many cases, tilt angles of 30° would be sufficient to turn the observed directions of motion into the line connecting the source

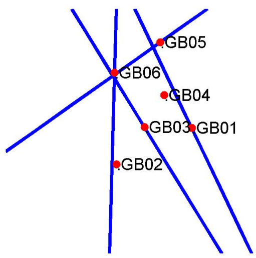

(a) Main direction of motion measured for an AA event

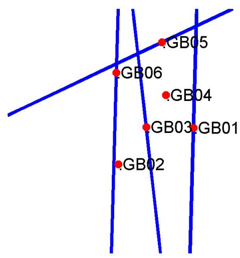

(b) Main direction of motion measured for an AA event

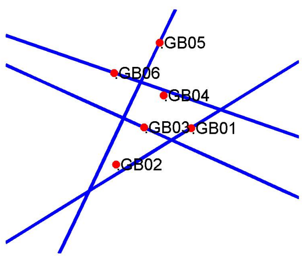

(c) Random ain directions

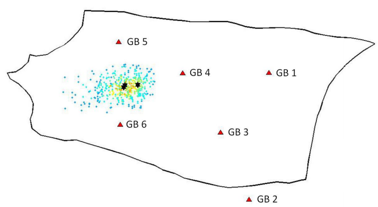

(d) Localization of the AA events shown in Figs. a.) to c.)

Figure 5.5.: Investigation of AA events

with the station. However, even higher deviations of the direction of motion with the true azimuth were observed in the case of the investigated rockfall events (no figures shown).

In addition to the measurement of the onset's main direction of motion, I tried to determine the timespan between the onset and the first time the main direction of motion was perpendicular to that at the onset. In the case of global earthquakes, this was a good measure for the time difference between the P- and the S-wave arrival. In the case of the investigated AA events, however, the resulting times did not show any recognizable correlation with the source distance as would be expected. Again, this might be due to the fact that in these short events the P- and S-wave do not properly split up or the arriving wave might actually be a superposition of surface waves.

The second class of events, I was especially interested in, were the class B events [26], since the occurrence of those was highly correlated with the beginning of the sliding period recorded. I hence analyzed 10 class B events dating from the 10th of may 2009 to the 27th of may 2009 using the complex covariance method with a time window of 1s. The only filters applied to this broad frequency data were the frequency-compensation explained earlier, a 1Hz high-pass filter and, if necessary, the notch filters also mentioned earlier. The majority of the class B events showed a stable apparent azimuth over the whole event, as can be seen in Figure 5.6. Note also the jump in the degree of polarization at the beginning of the event and the comparatively small ellipticity throughout its duration. This is a typical feature of all class B events analyzed dated between the 15th and the 20th of may 2009. The relatively high degree of polarization and the low ellipticity exposes the motion to be linear in nature. The main direction of motion is thereby given by the apparent azimuth. However, since we do not know which type of wave we are dealing with (P, S or Love-wave), the apparent azimuth cannot be related with the ray path's azimuth as was done in the P-wave analysis. In order to gain more information on the direction of motion, I averaged the

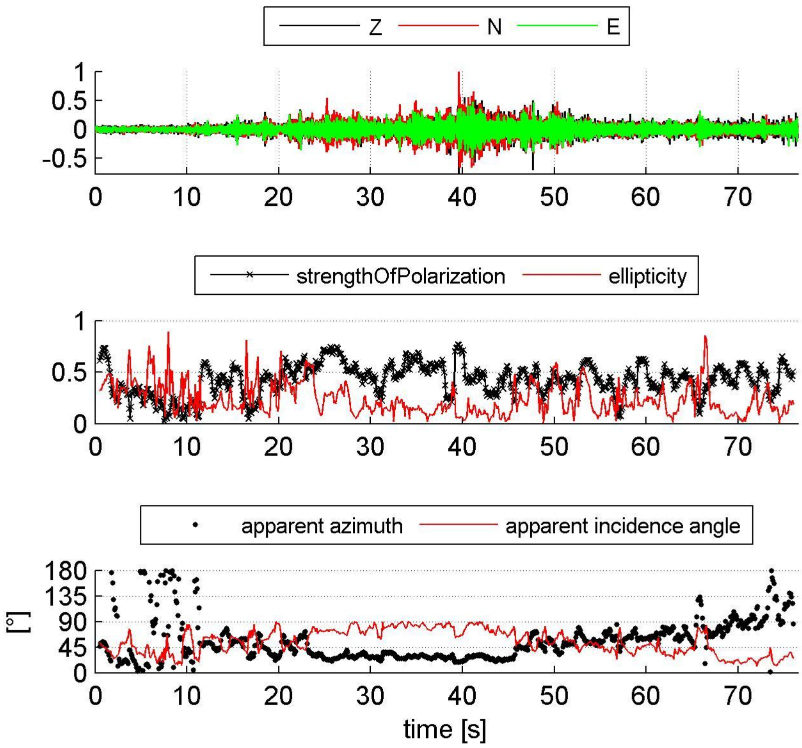

Figure 5.6.: Exemplary polarization of a class B event.

apparent azimuth over the whole time range, during which the azimuth was stable, the degree of polarization relatively high and the ellipticity low. This analysis brought a very interesting feature to light: All six class B events between the 15th and the 20th of may 2009 show, for each station, a similar direction of motion as can be seen in Figure 5.7. Class B events before or thereafter, however, show a different behavior (see Figure 5.7). This

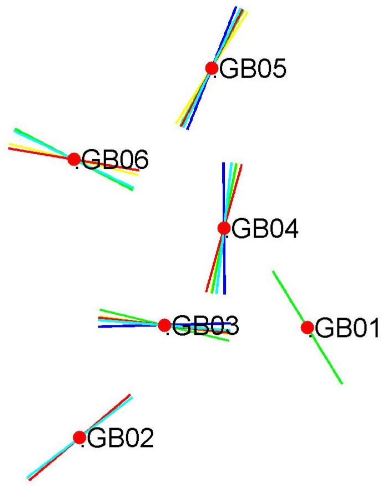

Figure 5.7.: Main direction of motion for class B events between 15th and 20th of may 2009.

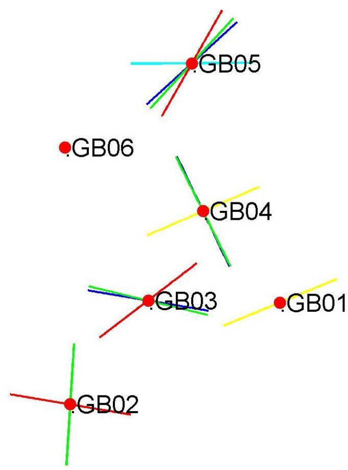

Figure 5.8.: Main direction of class B events between 10.5.2009 and 27.5.2009 omitting those events shown in Fig. 5.7. (blue line: before the 15th of may; all other lines: after the 20th of may.)

leads to the conclusion that there is, within the class B events, a subgroup of events that have, with a high probability, the same origin. This shows plainly that polarization analysis can be a useful tool when characterizing events. Whether the source is truly a sliding event remains open. In any case, the occurrence of class B events is correlated with the acceleration of the mass-movement, and the time between the 15th and 20th of may 2009 is a time of very strong acceleration. Figure 5.9. is result

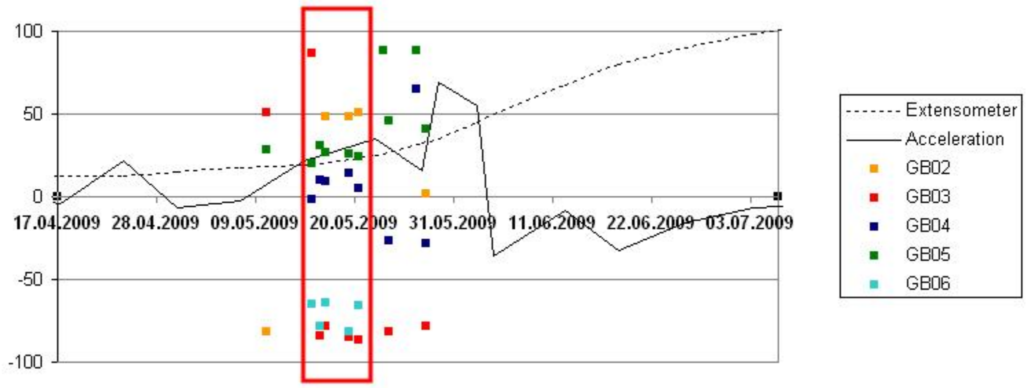

Figure 5.9.: Mass movement and its acceleration (in arb. units) and the measured apparent azimuth of class B events at stations in Gradenbach.

6. Conclusion

Within this work, I gave a state of the art review of different methods of polarization analysis used to analyze seismic data. Several methods were implemented in Seismon, tested on global earthquake data and applied to regional earthquake data and short period events.

The implemented methods include two covariance matrix methods, a complex covariance matrix method, a spectral matrix method and two methods relying on windowed Fourier transforms. Although the various methods do bare different information contents, many measures can be obtained by several methods. However, intelligently applying different methods also complementing information can be gained. This is especially true, when combining, for example, a covariance matrix method with the spectral matrix method. While the former is optimized to obtain a good time resolution, the latter gives spectral resolution. The spectral information can then be used - for example to design optimized filters (see for example Figures 4.4 and 4.5). The fine differences between the covariance matrix, the debiased covariance matrix method and the complex covariance matrix were discussed. The two first methods can be considered to be equivalent as long as frequency content not suited for the used time window is filtered. If this is not done, the debiased covariance method is advantageous. The complex covariance method is not so dependent on the interplay between the time window and the frequency content. A detailed discussion on the best time window to use (see Figures 4.10 and 4.11) shows the necessary trade off between time resolution and meaningfulness of the degree of polarization.

The Fourier transform related methods, the S-transform method and the STFT-method, are - due to the type of presentation - especially apt to identify Love and Rayleigh waves, as illustrated in Chapter 4.

Main advantages of the polarization analysis over re-orientation are the quantizability and the fact that the polarization analysis takes correlations between traces into account (see Section 4.4).

A detailed investigation showed that polarization analysis can even be used when dealing with complicated subsurface and surface structure as at the landslide in Gradenbach (see Section 5.3 and Figures 5.1 to 5.3). As a main measure, the P-wave's main direction of motion was used.

Trying to extract further information from short period events recorded at the landslide at Gradenbach proved difficult, but a main success could be obtained in improving the characterization of the class B events: A considerable subgroup of events of this class shows a very similar main directions of motion. In a future analysis it would be highly interesting if these directions can be used to infer informations about the sliding mechanism.

The full range of polarization analysis techniques introduced in this work allows for a much wider range of investigation than were performed here. Further investigations would therefore be desirable.

Bibliography

[1] E. A. Flinn. Signal analsis using rectilinearity and direction of particle motion. *Proceedings of the IEEE*, 53:1874–1876, 1965.

[2] D Clarke and J. F. Grainger. *Polarized light and Optical Measurement*. Pergamon Press, 1971.

[3] S. R. Cloude. *Polarisation*. Oxford University Press, 2010.

[4] E.R. Kanasewich, editor. *Time sequence analysis in geophysics*. The University of Alberta Press, 3rd edition, 1981.

[5] Jay Damask. *Polarization Optics in Telecommunications*. Springer, 2005.

[6] Igor B. Morozov and Scott B. Smithson. Instantaneous polarization attributes and directional filtering. *Geophysics*, 61(3):872–881, 1996.

[7] Panomsak Meemon, Mohamed Salem, Kye-Sung Lee, Maryam Chopra, and Jannick P. Rolland. Determination of the coherency matrix of a broadband stochastic electromagnetic light beam. *Journal of Modern Optics*, 55(17):2765–2776, 2008.

[8] R. Martinez-Herrero, P.M. Mejias, and G. Piquero. *Characterization of Partially Polarized Light Fields*. Springer, 2009.

[9] M. Schimmel and J. Gallart. The use of instantaneous polarization attributes for seismic signal detection and image enhancement. *Geophys. J. Int.*, 155(2):653–668, 2003.

[10] K. De Meersman, M. van der Baan, and J-M. Kendall. Signal extraction and automated polarisation analysis of mulit-component array data. *Bulletin of the Seismological Society of America*, 96:2415–2430, 2006.

[11] D. Praetorius, editor. *Numerische Mathematik*. Institut f¨ur Analysis und Scientific Computing Technische Universit¨at Wien, 2006.

[12] G.S. Wagner and T.J. Owens. Signal detection using multi-channel seismic data. *Bulletin of the Seismological Society of America*, 86(1A):221–231, 1996.

[13] J. E. Vidale. Complex polarization analsis of particle motion. *Bulletin of the Seismological Society of America*, 76(5):1393–1405, 1986.

[14] K. Bataille and J. M. Chiu. Polarization analysis of high-frequency three-component seismic data. *Bulletin of the Seismological Society of America*, 81(2):622–642, 1991.

[15] J.C Samson and J. V. Olson. Data-adaptive polarization filters for multichannel geophysical data. *Geophysics*, 46(10):1423–1431, 1981.

[16] J. Park, F. L. Vernen, and C. R. Lindberg. Frequency dependent polarization analysis of high-frequency seismograms. *Journal of Geophysical Research*, 92(B12):12664–12675, 1987.

[17] S. Hearn and N. Hendrick. A review of single-station time-domain polarisation analysis techniques. *J. Seism Explor.*, 8(2):181–202, 1999.

[18] B.L.N. Kennett. *The Seismic Wavefield*. Cambridge University Press, 2002.

[19] C. R. Pinnegar. Polarization analysis and polarization filtering of three-component signals with the time-frequency S transform. *Ge*, 165:596–606, 2006.

[20] R.G. Stockwell, L. Mansinha, and R.P. Lowe. Localization of the complex spectrum: the S-transform. *IEEE Transactions on Si*, 44(4):998–1001, 1996.

[21] Bulletin of the Zentralanstalt für Meteorologie und Geophysik, Austria.

[22] B. Alessandrini, M. Cattaneo, M. Demartin, M. Gasperini, and V.1994 Lanza. A simple P-wave polarization analysis: its application to earthquake location. *Annali di Geofisica*, 5:883–897, 1994.

[23] E. Brückl, F.K. Brunner, and K. Kraus. Kinematics of a deep-seated landslide derived from potogrammetric, GPS and geophysical data. *Engineering Geology*, 88:149–159, 2006.

[24] E. Brückl and J. Brückl. Geophysical models of the Lesachriegel and Gradenbach deep-seated mass-movements (schober range, austria). *Engineering Geology*, 83:254–272, 2006.

[25] D.I. Stefan Mertl, private communcation.

[26] E. Brückl, D. Binder, H. Hausmann, and S. Mertl. Hazard estimation of deep seated mass movements by microseismic monitoring. Final report, International Strategy for Hazard Reduction, 2008.

A. Derivations

A.1. Derivation of the Elliptical Equation from the Amplitude Vector

To derive the elliptical equations from the equation defining the amplitude vecor we start with the two parametric equations of Eq. (2.1):

$$E_\xi = A_\xi \cos(\omega t + \phi_\xi) = A_\xi \left[\cos(\omega t)\cos(\phi_\xi) - \sin(\omega t)\sin(\phi_\xi)\right] \tag{A.1}$$

$$E_\eta = A_\eta \cos(\omega t + \phi_\eta) = A_\eta \left[\cos(\omega t)\cos(\phi_\eta) - \sin(\omega t)\sin(\phi_\eta)\right] \tag{A.2}$$

Now we multiply the first equation with $\sin(\phi_\eta)$ and the second with $\sin(\phi_\xi)$ yielding

$$\frac{E_\xi}{A_\xi}\sin(\phi_\eta) = \cos(\omega t)\cos(\phi_\xi)\sin(\phi_\eta) - \sin(\omega t)\sin(\phi_\xi)\sin(\phi_\eta)$$
$$\frac{E_\eta}{A_\eta}\sin(\phi_\xi) = \cos(\omega t)\cos(\phi_\eta)\sin(\phi_\xi) - \sin(\omega t)\sin(\phi_\eta)\sin(\phi_\xi)$$

By subtracting the second equation from the first we obtain

$$\begin{aligned}\frac{E_\xi}{A_\xi}\sin(\phi_\eta) - \frac{E_\eta}{A_\eta}\sin(\phi_\xi) &= \cos(\omega t)\left[\cos(\phi_\xi)\sin(\phi_\eta) - \cos(\phi_\eta)\sin(\phi_\xi)\right] \\ &= \cos(\omega t)\sin(\phi_\eta - \phi_\xi)\end{aligned} \tag{A.3}$$

In a second step, we multiply Eq. (A.1) by $\cos(\phi_\eta)$ and Eq. (A.2) by $\cos(\phi_\xi)$:

$$\frac{E_\xi}{A_\xi}\cos(\phi_\eta) = \cos(\omega t)\cos(\phi_\xi)\cos(\phi_\eta) - \sin(\omega t)\sin(\phi_\xi)\cos(\phi_\eta)$$
$$\frac{E_\eta}{A_\eta}\cos(\phi_\xi) = \cos(\omega t)\cos(\phi_\eta)\cos(\phi_\xi) - \sin(\omega t)\sin(\phi_\eta)\cos(\phi_\xi)$$

As before, we subtract the equations, which leads to

$$\begin{aligned}\frac{E_\xi}{A_\xi}\cos(\phi_\eta) - \frac{E_\eta}{A_\eta}\cos(\phi_\xi) &= \sin(\omega t)\left[\sin(\phi_\xi)\cos(\phi_\eta) - \sin(\phi_\eta)\cos(\phi_\xi)\right] \\ &= -\sin(\omega t)\sin(\phi_\eta - \phi_\xi) \qquad \text{(A.4)}\end{aligned}$$

Now we square Eq. A.3 and Eq. A.4 and add them:

$$\frac{E_\xi^2}{A_\xi^2}\sin^2(\phi_\eta) + \frac{E_\eta^2}{A_\eta^2}\sin^2(\phi_\xi) - 2\frac{E_\xi E_\eta}{A_\xi A_\eta}\sin(\phi_\eta)\sin(\phi_\xi) = \cos^2(\omega t)\sin^2(\phi_\eta - \phi_\xi)$$
$$\frac{E_\xi^2}{A_\xi^2}\cos^2(\phi_\eta) + \frac{E_\eta^2}{A_\eta^2}\cos^2(\phi_\xi) - 2\frac{E_\xi E_\eta}{A_\xi A_\eta}\cos(\phi_\eta)\cos(\phi_\xi) = \sin^2(\omega t)\sin^2(\phi_\eta - \phi_\xi)$$

$$\frac{E_\xi^2}{A_\xi^2} + \frac{E_\eta^2}{A_\eta^2} - 2\frac{E_\xi E_\eta}{A_\xi A_\eta}\cos(\phi_\eta - \phi_\xi) = \sin^2(\phi_\eta - \phi_\xi)$$

This is the elliptic equation we wanted to derive.

B. User's Guide

In oder to have access to the polarization analysis tools and the processing tools implemented in the course of this work, pleas download the newest version of SEISMON from `http://www.stefanmertl.com/science` (You need to create an account to be able to download the software). Load or create a SEISMON project (see `http://www.stefanmertl.com/science/sdp/chunkedHtml/seismonBasics.html` for help). For the polarization analysis tools and for the rotating tools (see below for details), the data has have 3 components. To allow the identification of the three components, the *channel names* of the north, east and z component in the station file have to be `HHN` or `N`, `HHE` or `E` and `HHZ` or `Z`, respectively. If this is not the case you can add the keys used in a hard coded manner to the methods. This will be discussed in the appropriate sections.

B.1. Polarization Analysis

This user's guide is not intended to explain the methods implemented. Please refer to chapters 2 to 4 for this information. Instead, I will give a step by step introduction of how to access and use the polarization analysis tools implemented in the course of this work in SEISMON.

- Open a trace display (You have to display *all three components*). Filter and process the traces as you wish (under P-stack; edit); the polarization analysis tool will act on the processed traces (which are also shown in the trace display) and not on the original traces.

- Choose the polarization analysis method and the corresponding parameters you wish to use by selecting Analyze/Polarization Analysis/Edit Parameters from the drop down menus. A pop-up window will appear (see Figure B.1). You can choose the method from the drop-down menu.

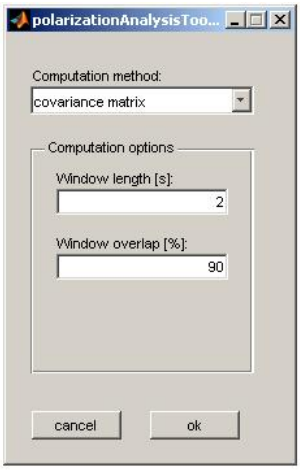

Figure B.1.: Pop-up window: Choose method and appropriate parameters.

  On choosing a method the corresponding parameters appear. Change the default-values shown to the desired values.

- Select Analyze/Polarization Analysis/run from the menus. Your cursor will change to a cross. Click and drag the cursor on any of the traces of the station you wish to analyze. The selected start and end point will be marked by a red line. A new window will open showing the result of the polarization analysis.

- In the polarization analysis window, you can once more change the method and the parameters used in the analysis. Choose Edit/Method from the polarization analysis' window menus and the Edit Parameters window will reappear. On clicking on OK, the new analysis will be performed and the plot will be updated.

Using channel names other than the standard names If your channel names are not `HHN` or `N`, `HHE` or `E` and `HHZ` or `Z` for the north, east and z component, respectively, you need to add your personal channel names to the program.

Open the file `\seismon\packages\pkg_trace_display\tools\+tool_polarizationAnalysis\windowButtonDownFcn.m` and change the following lines by adding your channel names to the appropriate struct.

```
%Define Keys for N, E, and Z direction
NKey={'HHN', 'N'};
ZKey={'HHZ', 'Z'};
EKey={'HHE', 'E'};
```

B.1.1. Additional features

From the covariance matrix method one additional feature can be accessed: The angle between the eigenvector corresponding to a specific time window and all other time windows can be displayed. To start this display, view the covariance matrix method and select a point in time within the uppermost axis displaying the traces (e.g. the onset of the P-wave). This will start the calculation of the angle between the eigenvector corresponding to the largest eigenvector in a time window starting at the selected point and a width equal to the time-window specified in the parameters of the covariance matrix method and the eigenvectors in the other time windows. The result is then displayed in the fourth axis of the updated plot. (See for example fig. 4.12). (The plot is titled “angle between p and current”. Note that this title is only correct if the time specified by clicking was the onset of the P-wave.)

B.2. Processing tools

In the process of this work, I implemented four different processing tools for SEISMON, namely, "rotate", "rotate to event", "resample" and "extend bandwidth". The action of the first three is quite clear. The first tool rotates the traces of all stations in the horizontal plane by one specified angle, the second tool rotates the traces of each station in the horizontal plane by the angle defined by the backazimuth of the station to the (previously specified) master event. "Resample" resamples the trace to a new (smaller) sampling rate (and applies an anti-aliasing filter first). The "extend bandwidth" method was written for the station at Gradenbach, which are 4Hz geophones. The algorithm is not yet flexible and will mathematically simulate an instrument response of 0.7Hz geophones instead of the 4Hz geophones.

B.2.1. Rotate

- Choose the processing stack from P-stack/edit
- Left click on "rotate" and select add from the drop-down menu. The processing node will appear on the left.
- Right click the processing node and select edid. Enter the angle in degrees by which you want to turn. The rotation direction is clockwise
- Click on OK.

B.2.2. Rotate to Event

- *Before* opening the processing stack, select a master event, by displaying the events and right-clicking on the the desired event and choosing set to master event.

- Now open the processing stack from P-stack/edit
- Left click on “rotate to event” and select add from the drop-down menu. The processing node will appear on the left.
- This is a non-editable node.

B.2.3. Resample

- Choose the processing stack from P-stack/edit
- Left click on “resample” and select add from the drop-down menu. The processing node will appear on the left.
- Right click the processing node and select edid. Enter desired sampling frequency in samples per second.
- Click on OK.

B.2.4. Rotate to Event

This tool will only affect stations called GB...

- O the processing stack from P-stack/edit
- Left click on “extend bandwidth” and select add from the drop-down menu. The processing node will appear on the left.
- This is a non-editable node.

Curriculum vitae

Name:	Katharina Doblhoff-Dier
Date of Birth:	13 May 1987
Nationality:	Austrian
Home address:	Döblinger Hauptstraße 64, 1190 Vienna, Austria

Education

06/2010:	Graduation diploma (MSc) in Technical Physics, Vienna University of Technology, Austria (passed with distinction)
2008-2009:	Study year abroad, University of Calgary, Canada (Grade point average: 4.0 out of 4.0)
2005-2010:	Study of Technical Physics, Vienna University of Technology, Austria
Since 2006:	Study of Geophysics, University of Vienna, Austria
01/2003-06/2003:	Term abroad, Wakefield Girls' High School, Wakefield, England
Since 1999:	Study of Violin, Vienna Music School

Research

currently:	PhD studies on the interaction of intense laser-fields with molecules, Institute for Theoretical Physics, Vienna University of Technology
12/2011-03/2011:	Diploma thesis (master's thesis) in geophysics: "Seismic signal analysis using polarization attributes and its applications", Institute of Geodesy and Geophysics, Vienna University of Technology

08/2010-11/2010: Project in theoretical attosecond science on attosecond streaking, Institute for Theoretical Physics, Vienna University of Technology

06/2009-05/2010: Diploma thesis (master's thesis) in technical physics: "Assessment of Technological Approaches for Exhaust Mass Flow Measurement Using Differential Pressure Devices", Institute of Applied Physics, Technical University of Vienna, in cooperation with AVL List Graz, Austria

01/2009-04/2009: Project work: "Spatio-temporal correlations in seismicit", Complexity Science Group, University of Calgary, Canada

09/2007: Project work: "Growth of platinum on platinum at low temperatures" in the field of surface physics, Institute for Applied Physics, Technical University of Vienna

07/2006: Internship at the German Aerospace Center, Germany

09/2005: Project work: "Analysis of the gene MAP65-3 in Arabidopsis Thaliana", Institute for Genetics and Cell Biology at the University of Natural Resources and Life Sciences, Vienna, Austria

Teaching Experience

3/2010-7/2010: Teaching Assistant for Statistical Physics I, Vienna University of Technology

10/2009-2/2010: Teaching Assistant for Quantum Physics I, Vienna University of Technology

Academic Awards and Grants

2010:	Gifted students grant for the academic year 2009/10
2008:	Joint Study grant awarded by the Vienna University of Technology for a study year in Canada
2007:	High potential program "TUtheTOP", Vienna University of Technology, Austria
2007:	Gifted students grant for the academic year 2006/07
2006:	Gifted students grant for the academic year 2005/06
2005:	Participation in the International Physics Olympiad

Publications in Refereed Journals

- T. P. Peixoto, K. Doblhoff-Dier, J. Davidsen:
  "Spatiotemporal correlations of aftershock sequences"
  Journal of Geophysical Research, 115, B10309 (2010).

- K. Doblhoff-Dier, K. Kudlaty, M. Wiesinger, M. Gröschl:
  "Time resolved measurement of pulsating flow using orifices"
  Flow Measurement and Instrumentation, 22, 2, p. 97-103 (2011).

- S. Nagele, R. Pazourek, J. Feist, K. Doblhoff-Dier, C. Lemell, K. Tökési, J. Burgdörfer:
  "Time-resolved photoemission by attosecond streaking: extraction of time information"
  Journal of Physics B, 44, 081001 (2011).